Title

Mapping the genome of meta-generalized gradient approximation density functionals: the search for B97M-V.

Journal

The Journal of chemical physics, 142(7)

ISSN

0021-9606

Authors

Mardirossian, Narbe
Head-Gordon, Martin

Publication Date

2015-02-01

DOI

10.1063/1.4907719

Peer reviewed

Mapping the genome of meta-generalized gradient approximation density functionals: The search for B97M-V

Narbe Mardirossian[†] and Martin Head-Gordon[*,†]

Kenneth S. Pitzer Center for Theoretical Chemistry, Department of Chemistry, University of California, Berkeley, California 94720, USA, and Chemical Sciences Division, Lawrence Berkeley National Laboratory, Berkeley, California 94720, USA

E-mail: mhg@cchem.berkeley.edu

Abstract

A meta-generalized gradient approximation (meta-GGA) density functional paired with the VV10 nonlocal correlation functional is presented. The functional form is selected from more than 10 billion choices carved out of a functional space of almost 10^{40} possibilities. Raw data comes from training a vast number of candidate functional forms on a comprehensive training set of 1095 data points and testing the resulting fits on a comprehensive primary test set of 1153 data points. Functional forms are ranked based on their ability to reproduce the data in both the training and primary test sets with minimum empiricism, and filtered based on a set of physical constraints and an often-overlooked condition of satisfactory numerical precision with medium-sized integration grids. The resulting optimal functional form has 4 linear exchange parameters, 4 linear same-spin correlation parameters, and 4 linear opposite-spin correlation parameters, for a total of 12 fitted parameters. The final density functional, B97M-V, is further assessed on a secondary test set of 212 data points, applied to several large systems including the coronene dimer and water clusters, tested for the accurate prediction of intramolecular and intermolecular geometries, verified to have a readily attainable basis set limit, and checked for grid sensitivity. Compared to existing density functionals, B97M-V is remarkably accurate for non-bonded interactions and very satisfactory for thermochemical quantities such as atomization energies, but inherits the demonstrable limitations of existing local density functionals for barrier heights.

[*]To whom correspondence should be addressed

[†]Kenneth S. Pitzer Center for Theoretical Chemistry, Department of Chemistry, University of California, Berkeley, California 94720, USA

[‡]Chemical Sciences Division, Lawrence Berkeley National Laboratory, Berkeley, California 94720, USA

1 Introduction

1.1 Perspective

Kohn-Sham density functional theory (KS-DFT)[1,2] is perhaps the most tractable approach to describing the electronic structure of molecules and solids in their ground state. The intractable, exact many-body wave function is replaced by a single determinant of spin orbitals, $\{\phi_i\}$, which describe a reference system of non-interacting electrons, whose density, $\rho(\mathbf{r})$, is to be the same as the interacting system of electrons under study. The single determinant of Kohn-Sham molecular orbitals is then used to represent the density, $\rho(\mathbf{r}) = \sum_i |\phi_i|^2$, as well as to evaluate the non-interacting kinetic energy.

The total energy, E_{tot}, is assembled from terms that can be exactly evaluated, and a remaining unknown term, E_{xc}, which is (in its simplest form) taken to be a functional of the electron density:

$$E_{tot} = -\sum_i \frac{1}{2} \left\langle \phi_i \left| \nabla^2 \right| \phi_i \right\rangle + \int \rho(\mathbf{r}) v_{ext}(\mathbf{r}) d\mathbf{r} + \frac{1}{2} \int \int \frac{\rho(\mathbf{r}_1)\rho(\mathbf{r}_2)}{r_{12}} d\mathbf{r}_1 d\mathbf{r}_2 + E_{nuc} + E_{xc} \quad (1)$$

The task of density functional development is to approximate E_{xc} as accurately as possible, while maintaining the computational tractability that characterizes the preceding 4 terms.

Since density functionals are models, there is no guarantee that a more complicated model will be more accurate than a simpler one. Nonetheless, if additional, physically-relevant information is incorporated into a density functional with minimal empiricism, it is certainly possible for the resulting density functional to improve upon a non-empirical density functional that excludes such information. This is the basis for systematically exploring semi-empirical density functionals that are increasingly complex functionals of the electron density. Following Perdew,[3] who assigned density functionals to various rungs of a ladder ascending from simplest to more complex (with more complex forms offering the possibility of satisfying additional exact conditions), one commonly identifies the following 5 rungs:

1. Local Spin-Density Approximation (LSDA): The LSDA exactly solves the infinite[4] uniform electron gas (UEG) problem and represents a non-empirical density functional that is the starting point for most of the following refinements. The exchange energy, as well as the same-spin and opposite-spin components of the correlation energy, are expressed in terms of an integral over the energy density per unit volume, $E_{x/c}^{LSDA} = \int e_{x/c}^{UEG}(\rho(\mathbf{r}))d\mathbf{r}$.

2. Generalized Gradient Approximation (GGA): Density functionals of this type enhance the LSDA energy density with an inhomogeneity correction factor (ICF), $g(s(\mathbf{r}))$, that depends on the reduced spin-density gradient, $s(\mathbf{r}) = \frac{\nabla\rho(\mathbf{r})}{\rho(\mathbf{r})^{4/3}}$, as in $E_{x/c}^{GGA} = \int e_{x/c}^{UEG}(\rho(\mathbf{r}))g_{x/c}(s(\mathbf{r}))d\mathbf{r}$. Leading GGAs include the non-empirical PBE density functional,[5] as well as the 9-parameter dispersion-corrected B97-D density functional[6].

3. Meta-Generalized Gradient Approximation (meta-GGA): In the early 1970s, while working on modeling nuclear matter forces, Negele and Vautherin[7] proposed the density matrix expansion (DME) in order to derive an approximate expression for the nuclear density matrix in terms of the nuclear density, its gradient, its Laplacian, and the nuclear kinetic energy density. More than 10 years later, Becke, using a similar approach, derived an approximate expression for the exchange charge density in terms of the electron density, its gradient, its Laplacian, as well as the electron kinetic energy density ($\tau = \sum_i^{occ.} |\nabla\phi_i|^2$). Since then, the term "meta-generalized gradient approximation"[8] (meta-GGA or MGGA) has come to signify density functionals that contain exchange or correlation components that depend on the kinetic energy density. As the central topic of this paper, existing meta-GGA density functionals will be reviewed in detail in Section 1.2.

4. Hybrid density functionals: Originally advocated by Becke,[9,10] hybrid density functionals evaluate a fraction of the exchange energy using the KS determinant as a wave function, leading to an explicit dependence upon the occupied KS orbitals. Such density functionals, beginning with B3PW91,[9,11,12] significantly improve upon Rung 2 and 3 density functionals for both thermochemical energy differences and reaction barriers, although the cost of evaluating exact ex-

change is a significant computational burden over local GGAs and meta-GGAs.

5. Double-hybrid density functionals (DHDF): DHDFs include dependence on the unoccupied KS orbitals in addition to the occupied levels, via either a second-order perturbation-like expression, or methods based on the random phase approximation. Such density functionals have demonstrated very high accuracy, albeit with significant additional computational demands beyond hybrids.

Even at Rung 2, and particularly at Rung 3 and higher, there is no unique way of designing non-empirical density functionals. Accordingly, semi-empirically-designed density functionals can compete effectively with those constructed from first principles. Recently, the systematic development of semi-empirical density functionals built upon the ICF of the global hybrid GGA density functional, B97, has been explored.[13] B97 expresses the ICFs for exchange, same-spin correlation, and opposite-spin correlation (g_x, g_{css}, and g_{cos}) as power series in a finite-range dimensionless variable, u, which in turn depends on the semi-infinite-range reduced spin-density gradient, s. Thus, each of the 3 ICFs can be expressed as:

$$g(u) = \sum_{j}^{M} c_j u^j \tag{2}$$

The aforementioned study first tested the comparative efficacy of different treatments of nonlocal exchange (none vs. global hybrid vs. range-separated hybrid) and nonlocal correlation (none vs. DFT-D2 vs. the VV10 nonlocal correlation (NLC) functional). Within the GGA framework, all of the functional forms from each of the 9 categories were assessed by considering all possible combinations of the approximately 15 parameters. The functional form which trained and tested best across 2301 data points spanning covalent and non-covalent interactions was deemed "optimal" in each category.

The overall winner from the 9 resulting "optimal" functional forms combined range-separation for nonlocal exchange with the VV10 NLC functional for the treatment of long-range dispersion interactions and was subsequently self-consistently trained. The result was a density functional with 7 linear parameters and 3 nonlinear parameters called ωB97X-V. For thermochemistry, ωB97X-V performed similarly to ωB97X-D, which has 13 linear parameters and 2 nonlinear parameters. However, it performed significantly more accurately for non-covalent interactions.

The question naturally arises as to whether a similar approach can be applied to the design of a Rung 3 density functional that uses the kinetic energy density as an additional variable. The primary goal of this paper is to answer this question. Since meta-GGAs are inherently more flexible than GGAs, the systematic exploration of the space of possible functional forms is considerably more difficult. Consequently, the challenge of systematic design is exponentially greater, because each of the one-dimensional power series expansions of Equation 2 must be replaced by two-dimensional expansions, where the new variable, w, depends on the kinetic energy density:

$$g(w,u) = \sum_{i}^{M'} \sum_{j}^{M} c_{ij} w^i u^j \tag{3}$$

In order to proceed, the maximum values of M and M' must be determined. Historically, most GGAs based on the B97 model have had success with values of M between 2 and 4. For the purposes of this study, M will be set to 4 and M' will be set to 8. With these choices ($M = 4$ and $M' = 2M = 8$), the search problem is of an enormous scale. The number of variables that can be individually included or excluded for each of the 3 components of the exchange-correlation energy is 44, assuming the UEG limit is enforced ($c_{00} = 1$). Under these conditions, the total number of possible functional forms is an astounding $2^{3\times44} = 2^{132} \sim 10^{40}$. The dimension of this space (10^{16} moles) is so enormous, that it is appropriate to label it the meta-GGA density functional genome.

An exhaustive search of the entire meta-GGA genome for the functional form which demon-

strates the highest degree of accuracy on training and test data is clearly impossible. Due to the scale of the problem, this functional search approach has not been previously extensively tried as a means of constructing a meta-GGA density functional (though a step in this direction has been recently reported for a meta-GGA exchange functional[14]). Nonetheless, this approach should be the goal of rational, semi-empirical density functional design, and an intelligent search of an interesting subspace can certainly be attempted. After reviewing the large number of existing meta-GGA density functionals and briefly summarizing dispersion corrections, the approach to attacking the search problem to design a new local meta-GGA density functional will be described.

1.2 meta-GGA Density Functionals

The first τ-dependent density functional was a same-spin correlation functional developed by Becke in 1985.[15] Several years later, Becke developed a more advanced, 2-parameter correlation functional (Bc88).[16] Bc88 had a τ-dependent same-spin correlation component due to a multiplicative factor (later termed the self-correlation correction (SCC) factor) that gave zero correlation energy for one-electron systems. Becke's first τ-dependent exchange functional, BR89, was developed in conjunction with Roussel,[17] and was modeled after the exchange hole of the hydrogen atom. Inspired by the SCC factor of the Bc88 correlation functional, Becke proposed a simpler, 2-parameter correlation functional (Bc95)[18] in 1995. Following the success of B97,[19] Becke developed the 10-parameter global hybrid meta-GGA density functional, B98.[20] Shortly after, Schmider and Becke[21,22] parameterized a series of B98-type density functionals on a variety of datasets in order to assess the sensitivity of the resulting empirical parameters to the training set. The inhomogeneity variable of B98 was slightly modified in 2000 with the B00 density functional[23] to give the w variable that would later become the backbone of most of Truhlar's exchange functionals.

Since the early 1990s, Proynov, Salahub, and coworkers have developed a series of τ-dependent correlation functionals, starting with LAP1 and LAP2,[24] which were based on the opposite-spin Colle-Salvetti pair-correlation function.[25] Soon thereafter, the LAP3 correlation functional[26] was developed in order to account for same-spin correlation. Its 4 parameters were fit in conjunction with an exchange functional (B88 for BLAP3 and PW86 for PLAP3) to a set of binding energies and bond lengths. The successor to LAP3, the τ1 correlation functional,[27] included higher-order τ-dependent terms, and its 5 parameters were fit in combination with a modified B88 exchange functional to give Bmτ1. Pairings of LAP3 and τ1 with the OPTX exchange functional,[28] OLAP3 and Oτ1, were later tested,[29] and Oτ2 was developed by refitting the parameters of both OPTX and τ1. Additionally,[30,31] TPSSτ1 assessed the pairing of TPSS exchange and τ1 correlation, while TPSSτ3 involved refitting the parameters of τ1 with TPSS exchange.

Koehl, Odom, and Scuseria (KOS) used the DME of Negele and Vautherin (NV)[7] to construct an exchange functional,[32] employing a more general coordinate system than NV. KOS were able to decrease the mean absolute deviation (MAD) of the exchange energies of 32 molecules more than 100-fold with a 2-parameter expression, giving the VT exchange functional. Van Voorhis and Scuseria (VS) showed that the exchange hole of VT diverged in the asymptotic limit and set out to ameliorate this problem,[33] as well as to add explicit dependence on the gradient of the density. The resulting 4-parameter GMVT and KMVT exchange functionals reduced the MAD of VT by another factor of 3 (to around 0.008 E_h). With 2 accurate exchange functionals, VS set out to develop a density functional[34] based on the DME. The resulting local meta-GGA density functional, VS98 (also known as VSXC or GVT4), had a total of 21 empirical parameters that were trained on atomization energies, ionization potentials, and bond lengths.

With only 1 empirical parameter, PKZB[8] was Perdew's first attempt at constructing a

local meta-GGA density functional. The exchange ICF of PKZB was an extension of that of the PBE exchange functional, albeit with a more complicated inhomogeneity variable that included kinetic energy density dependence, allowing for further constraint satisfaction. The PKZB correlation functional was similar to the PBE correlation functional, but was modified (with the help of τ) to return zero for one-electron densities (like Becke's SCC factor). PKZB was accurate for surface energies and atomization energies, but less satisfactory for hydrogen-bonded complexes and equilibrium bond lengths.[35] These problems were eventually attributed to shortcomings in the PKZB exchange functional, which was modified (along with minor improvements to the PKZB correlation functional) to yield the well-known, non-empirical local meta-GGA density functional, TPSS.[36] A 1-parameter global hybrid version of TPSS (TPSSh[37]) was developed shortly after, with 10% exact exchange. To improve TPSS atomization energies, modTPSS,[38] a 1-parameter version of TPSS which adjusted a previously fixed parameter in the exchange functional, was proposed. In 2009, a revised TPSS (revTPSS[39]) was introduced to overcome shortcomings in predicting accurate lattice constants, as well as to improve additional formal properties. The revTPSS exchange functional was altered to remedy an order of limits problem and paired with a modified PBE correlation functional to define the regTPSS density functional.[40] In 2012, Sun and coworkers[41] investigated the effect of the kinetic energy density on meta-GGA density functionals, which (along with the development of regTPSS) inspired the development of 4 local and 2 global hybrid meta-GGA density functionals:[41–45] MGGA_MS (MGGA_MS0), MGGA_MS1, MGGA_MS2, MGGA_MS2h, MVS, and MVSh.

Other groups were also active in proposing new meta-GGA density functionals in the early 2000s. The EDMGGA exchange functional[46] was based on the DME of the exchange hole and had an ICF that resembled that of B88, whilst using an inhomogeneity variable which depended (in part) on the kinetic energy density. A global hybrid variant[47] which combined EDMGGA with the Colle-Salvetti meta-GGA correlation functional[25,48] was also proposed, with 22% exact exchange. KCIS[49] was a meta-GGA correlation functional which depended on τ through its SCC term. KCIS was paired with various exchange functionals, including B88, PBE, and PKZB, and various global hybrid variants were also proposed, such as B0KCIS (25% exact exchange) and B1KCIS (23.9% exact exchange). Boese and Handy[50] based τ-HCTH on Becke's B97 and B98 density functionals. The same-spin and opposite-spin correlation ICFs used B97 expansions with $m = 3$. The exchange functional had both a "local" exchange component (B97-type with $m = 3$) and a "nonlocal" exchange component (Becke's 3-term B00 ICF[23] multiplying an $m = 3$ B97-type GGA ICF). τ-HCTH had 16 fitted parameters, while its global hybrid counterpart had 17 (with 15% exact exchange). BMK[51] was identical in form to the hybridized τ-HCTH, but since transition states were included in the training set (to better describe barrier heights), its percentage of exact exchange was almost 3 times larger (42%).

Between 2005 and 2011, Truhlar and coworkers have published 10 highly-parameterized local (M06-L,[52] M11-L[53]), global hybrid (M05,[54] M05-2X,[55] M06,[56] M06-2X,[56] M06-HF,[57] M08-HX,[58] M08-SO[58]), and range-separated hybrid (M11[59]) meta-GGA density functionals. The exchange component of M05 used the PBE exchange functional as its foundation, enhanced by a 12-term ($m = 11$) power series ICF in Becke's τ-dependent variable,[23] w, while the M05 correlation functional employed a 5-term B97-type expansion with Becke's SCC factor multiplying the same-spin component. All 3 UEG limits were satisfied, and a total of 22 fitted parameters (20 linear and 2 nonlinear) were optimized, including 28% exact exchange. The construction of M05-2X was identical to that of M05, except the exact exchange mixing parameter was doubled and fixed (56%) and the 2 nonlinear correlation parameters were borrowed from M05, for a total of 19 fitted parameters. The form of M06-L was an unhybridized M05 or M05-2X, with 1 exception:

all 3 components (exchange, same-spin correlation, and opposite spin correlation) had an additional, 5-term, VS98-type ICF. Since the nonlinear correlation parameters were borrowed from M05, M06-L ended up with a total of 34 fitted parameters. The global hybrid M06 density functional was identical to a hybridized M06-L, with 1 exception: the fourth-order terms from the VS98-type exchange ICF were dropped (2 fewer parameters). Accordingly, M06 had a total of 33 fitted parameters, with 27% exact exchange. M06-2X had double the amount of exact exchange (54%) as M06, and the entire VS98-type exchange ICF was dropped, resulting in 29 fitted parameters. M06-HF employed 100% exact exchange, and was otherwise identical to M06, with a total of 32 fitted parameters. M08-HX and M08-SO used exchange functionals based on the summation of the PBE and RPBE[60] ICFs, each enhanced by 12-term power series ICFs in w. For correlation, a third 12-term power series ICF in w enhanced the PW92 correlation energy density per unit volume and a fourth enhanced the PBE correlation functional gradient correction term. M08-HX involved 47 fitted parameters and 52.23% exact exchange, while for M08-SO, 3 additional constraints led to 44 fitted parameters and 56.79% exact exchange. The M11 density functional extended M08-HX and M08-SO with range-separated exact exchange and several minor changes, leading to 40 fitted parameters, 42.8% short-range exact exchange, and $\omega = 0.25$. The local meta-GGA density functional, M11-L, used a novel "dual-range" partitioning of the exchange functional, with a local "long-range" exchange component in addition to the short-range exchange component found in range-separated hybrid exchange functionals. The correlation functional was similar to that of M11, and all 6 power series (2 from SR exchange, 2 from LR exchange, and 2 from correlation) were reduced to 9 terms. With 54 initial linear parameters, 1 nonlinear parameter ($\omega = 0.25$), and 11 constraints, M11-L had a total of 44 fitted parameters.

Development of meta-GGAs continues actively to the present day. The meta-VT{8,4} exchange functional[61] was based on revTPSS, but differed in its inhomogeneity variable as well as its ICF, and was paired with the revTPSS correlation functional. ωM05-D was a dispersion-corrected, range-separated hybrid version[62] of Truhlar's M05 density functional with 21 fitted parameters, while ωM06-D3 represented similar modifications to Truhlar's M06-2X density functional and had 25 fitted parameters. These density functionals exhibited the advantages of range-separation and a correct treatment of long-range dispersion interactions. The BLOC exchange functional[63] was constructed by converting a constant in the TPSS and revTPSS exchange functionals to a function of the ratio of the von Weizsäcker kinetic energy density to the exact kinetic energy density. It was paired with the TPSSloc correlation functional[64] to give the BLOC density functional. Two density functionals have recently been developed within a Bayesian error estimation functional framework. BEEF-vdW[65] involved developing a 30-parameter GGA exchange functional and pairing it with 40% PBE correlation and 60% PW92 correlation, along with the vdW-DF-2 NLC functional.[66] This approach was naturally extended[14] to a 64-parameter meta-GGA exchange functional (mBEEF), which added the kinetic energy density as a variable, dropped the nonlocal correlation functional, and replaced the combination of PBE correlation and PW92 correlation with the PBEsol correlation functional.[67]

1.3 van der Waals Interactions

Since long-range electron correlations that account for the asymptotic $1/r^6$ dependence of van der Waals (vdW) interactions cannot be properly described by conventional density functionals,[68,69] there has been an increased effort in the past decade to remedy this shortcoming. While numerous methods that account for dispersion have been proposed, this brief review is limited to the DFT-D approach of Grimme[6,70,71] and the nonlocal correlation functionals of Lundqvist and Van Voorhis.[66,72–78] A comprehensive review of various approaches to extending the applicability

of DFT to dispersion interactions can be found in Reference 79.

The simplest and cheapest methods that account for dispersion are Grimme's empirical DFT-D methods,[6,70,71] which are damped interatomic potentials. Grimme's first attempt at an empirical dispersion tail was DFT-D1,[70] which was only available for 6 elements (H, C, N, O, F, and Ne). With the atomic C_6 parameters and van der Waals radii predetermined, a single linear optimizable parameter (s_6) was trained onto 3 existing local GGA density functionals (BLYP, BP86, and PBE) and led to a considerable improvement in the description of vdW interactions. Grimme then introduced the DFT-D2 dispersion tail for all elements through Xe, along with a 9-parameter, B97-based, local GGA density functional called B97-D. Independent damping parameters were determined for PBE, BLYP, BP86, TPSS, and B3LYP. This was followed by the DFT-D3 dispersion tail, which used fractional coordination numbers to account for variations in atomic dispersion coefficients in different chemical environments and contained a two-body term and an optional three-body term, with an improved damping function. The DFT-D3 dispersion tail was trained onto more than 10 existing density functionals and generally improved upon its predecessors for describing dispersion interactions.

Several density functionals that explicitly account for dispersion have been developed, including vdW-DF-04,[72] vdW-DF-10,[66] VV09,[74] and VV10.[76] These nonlocal correlation functionals rely on a double space integral over the density and a nonlocal correlation kernel, and are computationally more expensive than the DFT-D methods. Langreth, Lundqvist, and coworkers introduced the first NLC scheme (vdW-DF-04) that could be applied to overlapping densities in 2004. Several years later, Vydrov and Van Voorhis implemented the vdW-DF-04 NLC functional for use with Gaussian basis sets,[73] and proposed modifications (vdW-DF-09) to improve its compatibility with existing exchange functionals.[75] The VV09[74,77,78] NLC functional of Vydrov and Van Voorhis adopted a simple analytic form for the nonlocal correlation kernel, instead of relying on a numerically tabulated kernel. Soon afterwards, Vydrov and Van Voorhis proposed an even simpler NLC functional, VV10, that improved upon its predecessor by employing a less elaborate function for the damping of the $1/r^6$ asymptote. In 2010, vdW-DF-10 was introduced to correct the tendency of vdW-DF-04 to overestimate equilibrium bond lengths and underestimate the binding energies of hydrogen-bonded complexes. While the vdW-DF methods have no optimizable parameters, VV09 and VV10 have 1 and 2 optimizable parameters, respectively.

1.4 Outline

This paper describes the task of designing an accurate and computationally efficient local meta-GGA density functional by attempting a partial search of the functional space defined by the inclusion or exclusion of the parameters in Equation 3. To ensure computational efficiency, B97M-V will not include exact exchange; i.e. it is semilocal as far as exchange is concerned. This will impose some limits on the accuracy of B97M-V for properties such as barrier heights that are sensitive to the inclusion of exact exchange. To offer the possibility of high accuracy for non-covalent interactions, particularly in the asymptotic regime, B97M-V will include nonlocal correlation via the VV10 NLC functional, which has already been demonstrated to be highly effective for this purpose[76] and is computationally efficient.

The remainder of the paper is organized as follows. Details of the methodology used are discussed in Section 2, beginning with a full specification of the functional forms that are being trained and tested, followed by details regarding the choice of basis sets and grids, and a brief summary of the datasets that will be employed for training and testing B97M-V. Most importantly, Section 2.5 describes the way in which a partial search of the meta-GGA density functional genome (from which B97M-V was drawn) was attempted. Since the inclusion of the kinetic energy density is known to lead to oscillations in potential energy curves

for weakly interacting systems (i.e. strong integration grid sensitivity), this aspect was heavily emphasized in the development of B97M-V.

The functional form of B97M-V emerged as the leading representative of the "fittest" functional forms encountered in the search. Having selected a functional form, B97M-V was then self-consistently trained and assessed against a broad range of existing density functionals in Section 3. These assessments begin with the training and test data from which B97M-V emerged, and then progress to a range of further tests on data which was not used for developing or selecting B97M-V.

2 Approach

2.1 Theory

The complete functional form for B97M-V is given by Equation 4. The components of the exchange functional and correlation functional are described below. The acronyms used in Equation 4 (and henceforth) are: exchange-correlation (xc), exchange (x), correlation (c), same-spin (ss), and opposite-spin (os).

$$E_{xc}^{B97M-V} = E_{x}^{B97M-V} + E_{css}^{B97M-V} + E_{cos}^{B97M-V} + E_{NLC}^{VV10} \tag{4}$$

The local spin-density approximation (LSDA) for exchange can be expressed in terms of the first-order spinless reduced density matrix for a uniform electron gas (UEG):

$$E_{x}^{LSDA} = -\frac{1}{2}\sum_{\sigma}^{\alpha,\beta}\int\int\frac{1}{s}|\rho_{\sigma}^{UEG}(\mathbf{r},s)|^{2}d\mathbf{r}d\mathbf{s} \tag{5}$$

$$\rho_{\sigma}^{UEG}(\mathbf{r},s) = 3\rho_{\sigma}(\mathbf{r})\left[\frac{\sin(k_{F\sigma}s) - k_{F\sigma}s\cos(k_{F\sigma}s)}{\left[k_{F\sigma}s\right]^{3}}\right] \tag{6}$$

where $\mathbf{s} = \mathbf{r}_1 - \mathbf{r}_2$, $\mathbf{r} = \frac{1}{2}\left[\mathbf{r}_1 + \mathbf{r}_2\right]$, and $k_{F\sigma} = \left[6\pi^2\rho_{\sigma}\right]^{1/3}$ is the spin-polarized Fermi wave vector. Integration of Equation 5 over $\mathbf{s}$ gives the well-known expression for the LSDA exchange energy in terms of the exchange energy density per unit volume of a uniform electron gas:

$$E_{x}^{LSDA} = \sum_{\sigma}^{\alpha,\beta}\int e_{x,\sigma}^{UEG}(\rho_{\sigma})d\mathbf{r} \tag{7}$$

$$e_{x,\sigma}^{UEG}(\rho_{\sigma}) = -\frac{3}{2}(\frac{3}{4\pi})^{1/3}\rho_{\sigma}^{4/3} \tag{8}$$

Accounting for inhomogeneities in the electron density is achieved by multiplying the integrand of the LSDA exchange functional by a power series inhomogeneity correction factor, $g_x(w_{x,\sigma}, u_{x,\sigma})$, resulting in the B97M-V exchange functional:

$$E_{x}^{B97M-V} = \sum_{\sigma}^{\alpha,\beta}\int e_{x,\sigma}^{UEG}(\rho_{\sigma})g_{x}(w_{x,\sigma},u_{x,\sigma})d\mathbf{r} \tag{9}$$

$$g_{x}(w_{x,\sigma},u_{x,\sigma}) = \sum_{i=0}\sum_{j=0}c_{x,ij}w_{x,\sigma}^{i}u_{x,\sigma}^{j} \tag{10}$$

$$w_{x,\sigma} = \frac{t_{\sigma}-1}{t_{\sigma}+1} \tag{11}$$

$$u_{x,\sigma} = \frac{\gamma_{x}s_{\sigma}^{2}}{1+\gamma_{x}s_{\sigma}^{2}} \tag{12}$$

where the dimensionless variable, $w_{x,\sigma} \in [-1,1]$, is a finite domain transformation of the ratio of the UEG kinetic energy density to the exact kinetic energy density, $t_{\sigma} = \frac{\tau_{\sigma}^{UEG}}{\tau_{\sigma}}$, with $\tau_{\sigma}^{UEG} = \frac{3}{5}(6\pi^2)^{\frac{2}{3}}\rho_{\sigma}^{\frac{5}{3}}$, and the dimensionless variable, $u_{x,\sigma} \in [0,1]$, is a finite domain transformation of the reduced spin-density gradient, $s_{\sigma} = \frac{|\nabla\rho_{\sigma}|}{\rho_{\sigma}^{4/3}} \in [0,\infty)$. The linear DFT exchange parameters, $c_{x,ij}$, will be determined by least-squares fitting to a training set in Section 2.5, while $\gamma_x = 0.004$ is a nonlinear DFT exchange parameter that was fit to the Hartree–Fock exchange energies of 20 atoms in 1986 by Becke.[80]

Closed-form expressions for the correlation energy density per particle of a uniform electron gas, $\epsilon_{c}^{UEG}(\rho)$, are only known for the low- and high-density limits of the paramagnetic and ferromagnetic cases of the UEG. Using the Monte-Carlo data of Ceperley and Alder,[81] Perdew and Wang developed an analytic spin-compensated representation,[82] $\epsilon_{c}^{PW92}(\rho)$, for $\epsilon_{c}^{UEG}(\rho)$. Combined with the spin-polarization interpolation formula of Vosko, Wilk, and Nusair,[83] the spin-polarized PW92 correlation energy density per particle, $\epsilon_{c}^{PW92}(\rho_{\alpha},\rho_{\beta})$, is the starting point for the B97M-V correlation func-

tional:

$$E_c^{LSDA} = \int \rho \epsilon_c^{PW92}(\rho_\alpha, \rho_\beta) d\mathbf{r} \tag{13}$$

Using the spin decomposition technique of Stoll and coworkers,[84] the LSDA correlation energy can be separated into same-spin and opposite-spin components:

$$E_{css}^{LSDA} = \sum_{\sigma}^{\alpha,\beta} \int e_{c,\sigma\sigma}^{PW92} d\mathbf{r} = \int \rho_\alpha \epsilon_c^{PW92}(\rho_\alpha, 0) d\mathbf{r} + \int \rho_\beta \epsilon_c^{PW92}(0, \rho_\beta) d\mathbf{r} \tag{14}$$

$$E_{cos}^{LSDA} = \int e_{c,\alpha\beta}^{PW92} d\mathbf{r} = \int \rho \epsilon_c^{PW92}(\rho_\alpha, \rho_\beta) d\mathbf{r} - \int \rho_\alpha \epsilon_c^{PW92}(\rho_\alpha, 0) d\mathbf{r} - \int \rho_\beta \epsilon_c^{PW92}(0, \rho_\beta) d\mathbf{r} \tag{15}$$

where $e_{c,\sigma\sigma}^{PW92}$ and $e_{c,\alpha\beta}^{PW92}$ are the PW92 same-spin and opposite-spin correlation energy densities per unit volume. Extending Equations 14 and 15 to account for inhomogeneities in the electron density is straightforward, since the same approach used for the exchange functional can be utilized:

$$E_{css}^{B97M-V} = \sum_{\sigma}^{\alpha,\beta} \int e_{c,\sigma\sigma}^{PW92} g_{css}(w_{c,\sigma\sigma}, u_{c,\sigma\sigma}) d\mathbf{r} \tag{16}$$

$$g_{css}(w_{c,\sigma\sigma}, u_{c,\sigma\sigma}) = \sum_{i=0} \sum_{j=0} c_{css,ij} w_{c,\sigma\sigma}^i u_{c,\sigma\sigma}^j \tag{17}$$

$$w_{c,\sigma\sigma} = \frac{t_\sigma - 1}{t_\sigma + 1} \tag{18}$$

$$u_{c,\sigma\sigma} = \frac{\gamma_{css} s_\sigma^2}{1 + \gamma_{css} s_\sigma^2} \tag{19}$$

$$E_{cos}^{B97M-V} = \int e_{c,\alpha\beta}^{PW92} g_{cos}(w_{c,\alpha\beta}, u_{c,\alpha\beta}) d\mathbf{r} \tag{20}$$

$$g_{cos}(w_{c,\alpha\beta}, u_{c,\alpha\beta}) = \sum_{i=0} \sum_{j=0} c_{cos,ij} w_{c,\alpha\beta}^i u_{c,\alpha\beta}^j \tag{21}$$

$$w_{c,\alpha\beta} = \frac{t_{\alpha\beta} - 1}{t_{\alpha\beta} + 1} \tag{22}$$

$$u_{c,\alpha\beta} = \frac{\gamma_{cos} s_{\alpha\beta}^2}{1 + \gamma_{cos} s_{\alpha\beta}^2} \tag{23}$$

where $t_{\alpha\beta} = \frac{1}{2}(t_\alpha + t_\beta)$ and $s_{\alpha\beta}^2 = \frac{1}{2}(s_\alpha^2 + s_\beta^2)$. The linear DFT correlation parameters, $c_{css,ij}$ and $c_{cos,ij}$, will be determined by least-squares fitting to a training set in Section 2.5, while $\gamma_{css} = 0.2$ and $\gamma_{cos} = 0.006$ are nonlinear DFT correlation parameters that were fit to the correlation energies of neon and helium in 1997 by Becke.[19]

Nonlocal correlation is taken into account via the VV10 NLC functional:[76]

$$E_{NLC}^{VV10} = \int \rho(\mathbf{r}) \left[\frac{1}{32} \left[\frac{3}{b^2} \right]^{3/4} + \frac{1}{2} \int \rho(\mathbf{r}') \Phi(\mathbf{r}, \mathbf{r}', \{b, C\}) d\mathbf{r}' \right] d\mathbf{r} \tag{24}$$

where $\Phi(\mathbf{r}, \mathbf{r}', \{b, C\})$ is the nonlocal correlation kernel defined in Reference 76. The VV10 NLC functional introduces 2 nonlinear parameters: b, which controls the short-range damping of the $1/r^6$ asymptote, and C, which controls the accuracy of the asymptotic C_6 coefficients.

2.2 Datasets

A semi-empirical density functional is only as applicable as the data used to train and test it. In total, the training, primary test, and secondary test sets contain 2460 data points, requiring 2421 single-point calculations. Of the 2460 data points, 1095 belong to the training set, 1153 belong to the primary test set, and 212 belong to the secondary test set. Furthermore, the training, primary test, and secondary test sets contain both thermochemistry (TC) data as well as non-covalent interactions (NC) data. The training set contains 787 TC data points and 308 NC data points, the primary test set contains 134 TC data points and 1019 NC data points, and the secondary test set contains 81 TC data points and 131 NC data points (for an overall total of 1002 TC data points and 1458 NC data points). Table 1 lists the 45 datasets that form the training, primary test, and secondary test sets. Specific details regarding the datasets can be found in Section 4 of Reference 85, with the only difference being that updated reference values for HW6F, HW6Cl, and H2O6Bind8 are used in this work.[86]

Table 1: Summary of the datasets found in the training, primary test, and secondary test sets. The datasets above the first thick black line are in the training set, the datasets between the first and second thick black lines are in the primary test set, while the datasets below the second thick black line are in the secondary test set. Within the training, primary test, and secondary test sets, datasets above the thin black line contain thermochemistry (TC) data points, while datasets below the thin black line contain non-covalent interactions (NC) data points. PEC stands for potential energy curve.

Name	Description	# of Data Points	References
HAT707	Heavy-atom transfer reaction energies	505	87
BDE99	Bond dissociation reaction energies	83	87
TAE_nonMR124	Total atomization energies (nonmultireference)	124	87
SN13	Nucleophilic substitution reaction energies	13	87
ISOMER20	Isomerization reaction energies	18	87
DBH24	Diverse barrier heights	24	88,89
EA6	Electron affinities of atoms	6	90
IP6	Ionization potentials of atoms	6	90
AE8	Absolute atomic energies	8	91
SW49Rel345	$SO_4{}^{2-}(H_2O)_n$ ($n = 3-5$) relative energies	28	92
SW49Bind345	$SO_4{}^{2-}(H_2O)_n$ ($n = 3-5$) binding energies	30	92
NBC10-2	Methane dimer and benzene-methane dimer PECs	37	93,94
BzDC215	Benzene and first- and second-row hydride PECs	108	95
NBC10-1	Parallel-displaced (3.4 Å), sandwich, and T-shaped benzene dimer PECs	53	93,94
HW30	Hydrocarbon and water dimers	30	96
S22	Equilibrium geometries from S22x5	22	94,97
EA7	Adiabatic electron affinities of small molecules	7	90
IP7	Adiabatic ionization potentials of small molecules	7	90
AlkAtom19	$n = 1-8$ alkane atomization energies	19	98
AlkIsomer11	$n = 4-8$ alkane isomerization energies	11	98
AlkIsod14	$n = 3-8$ alkane isodesmic reaction energies	14	98
HTBH38	Hydrogen transfer barrier heights	38	99
NHTBH38	Non-hydrogen transfer barrier heights	38	100
SW49Rel6	$SO_4{}^{2-}(H_2O)_n$ ($n = 6$) relative energies	17	92
SW49Bind6	$SO_4{}^{2-}(H_2O)_n$ ($n = 6$) binding energies	18	92
HBC6	Formic acid, formamide acid, and formamidine acid dimer PECs	118	94,101
NBC10-3	S2 and T3 configuration pyridine dimer PECs	39	94,102
S22x5	Hydrogen-bonded and dispersion-bound complex PECs	110	103
S66x8	Biomolecular structure complex PECs	528	104
S66	Equilibrium geometries from S66x8	66	104,105
NNTT41	Neon-neon PEC	41	106
AATT41	Argon-argon PEC	41	106
NATT41	Neon-argon PEC	41	106
G21EA	Adiabatic electron affinities of atoms and small molecules	25	107,108
G21IP	Adiabatic ionization potentials of atoms and small molecules	36	107,108
PA8	Adiabatic proton affinities of small molecules	8	109,110
Gill12	Neutral, radical, anionic, and cationic isodesmic reaction energies	12	111
A24	Small non-covalent complexes	24	112
X40	Non-covalent interactions of halogenated molecules	40	113
H2O6Bind8	Binding energies of water hexamers	8	86,114
HW6F	Binding energies of $F^-(H_2O)_n$ ($n = 1-6$)	6	86,114
HW6Cl	Binding energies of $Cl^-(H_2O)_n$ ($n = 1-6$)	6	86,114
CYCONF	Relative energies of cysteine conformers	10	108,115
DS14	Binding energies for complexes containing divalent sulfur	14	116
WATER27	Neutral and charged water interactions	23	108,117

2.3 Computational Details

For the training, primary test, and secondary test sets, the (99,590) grid (99 radial shells with 590 Lebedev points each) was used to evaluate local exchange-correlation (xc) functionals, while the SG-1 grid[118] was used to evaluate the VV10 NLC functional. For the absolute atomic energies in the training set and the rare-gas dimer PECs in the primary test set, the (500,974) grid was used to evaluate local xc functionals, while the (99,590) grid was used to evaluate the VV10 NLC functional. For M06-L and M11-L, calculations in the training, primary test, and secondary test sets were carried out with the (250,590) grid instead of the (99,590) grid. For the sake of simplicity, the following convention will be used henceforth: the grid used to integrate the local xc functional will be appended with a forward slash, followed by the grid used to integrate the VV10 NLC functional (if applicable). Therefore, referring to the second sentence of this paragraph, it will suffice to state that the (500,974)/(99,590) grid was used for the absolute atomic energies and the rare-gas dimer PECs.

The aug-cc-pVQZ (aQZ) basis set[119,120] was used for all thermochemistry data points in the training, primary test, and secondary test sets except the second-row absolute atomic energies in the training set (aug-cc-pCVQZ),[119,120] while the aug-cc-pVTZ (aTZ) basis set[119,120] was used for all non-covalent interactions data points in the training, primary test, and secondary test sets except the rare-gas dimer PECs in the primary test set (aQZ) and the X40 dataset in the secondary test set (def2-TZVPPD[121,122]). All non-covalent interactions were computed *without* counterpoise corrections (unless otherwise noted).

For B97-D2, Grimme's DFT-D2 dispersion tail was used with an s_6 coefficient of 0.75, as parameterized by Burns and coworkers.[123] Grimme's B97-D density functional[6] uses the DFT-D2 dispersion tail as well, with an s_6 coefficient of 1.25. For B3LYP-D3, Grimme's DFT-D3 dispersion tail was used with the following set of parameters: $\{s_6,\, s_{r,6},\, s_8,\, s_{r,8}\} = \{1,\, 1.261,\, 1.703,\, 1\}$. For PBE-D3, Grimme's DFT-D3 dispersion tail was used with the following set of parameters: $\{s_6,\, s_{r,6},\, s_8,\, s_{r,8}\} = \{1,\, 1.217,\, 0.722,\, 1\}$. For TPSS-D3, Grimme's DFT-D3 dispersion tail was used with the following set of parameters: $\{s_6,\, s_{r,6},\, s_8,\, s_{r,8}\} = \{1,\, 1.166,\, 1.105,\, 1\}$. The density functionals that utilize the DFT-D3 dispersion tail use its zero-damping implementation (commonly referred to as DFT-D3(0)). Electronic energies are exclusively used throughout this paper and spin-orbit coupling is not taken into consideration. All of the calculations were performed with a development version of Q-Chem 4.0.[124]

2.4 Least-Squares Procedure

With a total of 2248 data points in the training and primary test sets, it is clear that a comprehensive 2-parameter nonlinear optimization of the parameters associated with VV10 is impractical. As a result, the values of $b = 6$ and $C = 0.01$ that were optimized for ωB97X-V are taken without further adjustment.

For the least-squares fits associated with the development of B97M-V, 1880 molecules comprise the 2248 data points in the training and primary test sets. The molecular orbital (MO) coefficients for these 1880 molecules were initially converged with the LSDA+VV10 density functional and saved to disk (equivalent to $g_x = g_{css} = g_{cos} = 1$). Using these saved MO coefficients, the values (henceforth referred to as contributions) that are enhanced by the exchange ($c_{x,ij}$), same-spin correlation ($c_{css,ij}$), and opposite-spin correlation ($c_{cos,ij}$) coefficients are computed up to 8th order in w and up to 4th order in u (including cross terms) for a total of 135 contributions per molecule, to enable the evaluation of Equation 3. These values are computed twice: once with the (99,590)/SG-1 grid and once with the (250,590)/SG-1 grid (the (500,974)/(99,590) grid was always used for AE8, NNTT41, AATT41, and NATT41 throughout this paper and never altered).

The contributions are used to form a (# of data points) $\times$ (# of linear parameters) matrix, A. In addition to the A matrix, a column vector, y, of values corresponding to the

errors in the unoptimized density functional ($y = E_{REF} - E_{DFT}$) is computed. Since weights are used during training, a diagonal (# of data points) × (# of data points) training set weight matrix (W_{Train}) is required as well. The diagonal elements corresponding to the training set data contain the appropriate weights, while the remaining diagonal elements corresponding to the primary test set data are set to zero. Thermochemistry data points in the training and primary test sets are given weights of 1 and 2, respectively (except for data points in TAE_nonMR124 (5), EA6 (10), IP6 (10), and DBH24 (25)), non-covalent interactions data points in the training and primary test sets are given weights of 100 and 200, respectively, and data points corresponding to the rare-gas dimer potential energy curves (PEC) in the primary test set are given a weight of 100,000. The total root-mean-square deviation (RMSD) is defined as a weighted RMSD of all 2248 data points in the training and primary test sets with the aforementioned weights, while the training RMSD is defined as a weighted RMSD of the 1095 data points in the training set with the aforementioned weights.

The change in the linear parameters, Δb, is found by a weighted least-squares fit:

$$\Delta b = (A^T W_{Train} A)^{-1} (A^T W_{Train} y) \qquad (25)$$

Unless otherwise noted, Δb is computed using the data generated with the (250,590)/SG-1 grid. The training set RMSD is calculated by:

$$RMSD_{Train} = \sqrt{\frac{\mathrm{diag}(W_{Train}) \cdot (y - A\Delta b)^2}{\#_{Train}}} \qquad (26)$$

while the total RMSD is calculated by:

$$RMSD_{Total} = \sqrt{\frac{\mathrm{diag}(W_{Total}) \cdot (y - A\Delta b)^2}{\#_{Total}}} \qquad (27)$$

With the contributions calculated with 2 different grids, it is straightforward to analyze the energetic differences between the grids per contribution per data point. Figure 1 plots the difference between the (99,590)/SG-1 data and (250,590)/SG-1 data for each of the 135 contributions for all 2248 data points. As a reminder, grid-based errors involve the product of these differences and the corresponding coefficient that appears in the density functional. For instance, the largest grid-based error (-0.0195 kcal/mol for the parallel-displaced benzene dimer from S22x5 at 0.9·R_e) comes from $u_{c,\sigma\sigma}$, and a well-behaved density functional like ωB97X-V has $c_{css,01} = -0.274$, meaning that the resulting error is only 0.00533 kcal/mol. More attention should be paid to higher-order variables, because while their grid-based errors might seem small, such terms are more likely to have large coefficients. For example, M06-L has $c_{cos,02} = -251.325$, and the largest error for the associated variable is -0.000622 kcal/mol, which leads to a more significant total error of 0.156 kcal/mol. However, since grid-based errors might cancel upon integration, fits are not discarded solely based on the magnitude of the resulting coefficients. The procedure used to ensure that the final density functional is as grid-insensitive as possible will be discussed in the following section.

2.5 Partial Search of the Functional Space

Following the initial setup described above, a subspace of the full parameter space must be selected to begin the search. The initial parameter space consists of 135 parameters. With the available computing resources (a dedicated 64-core node), the maximum number of fits that can be performed in a single day is around 2 billion. Therefore 135C5 is the largest 1-day calculation that can be performed with all 135 parameters, resulting in only up to 5-parameter fits. A prior search of the much smaller GGA parameter space to design ωB97X-V led to an optimal functional form with a total of 7 linear parameters, but since τ-dependent variables are being included in this fit, larger numbers of parameters are almost certainly required. To reduce the size of the search space, certain higher-order variables are excluded: only contributions from variables up to combined 6th order ($u + w$) are included in the fits. Furthermore, all 3 uniform electron gas limits are satisfied, further reducing the total number of

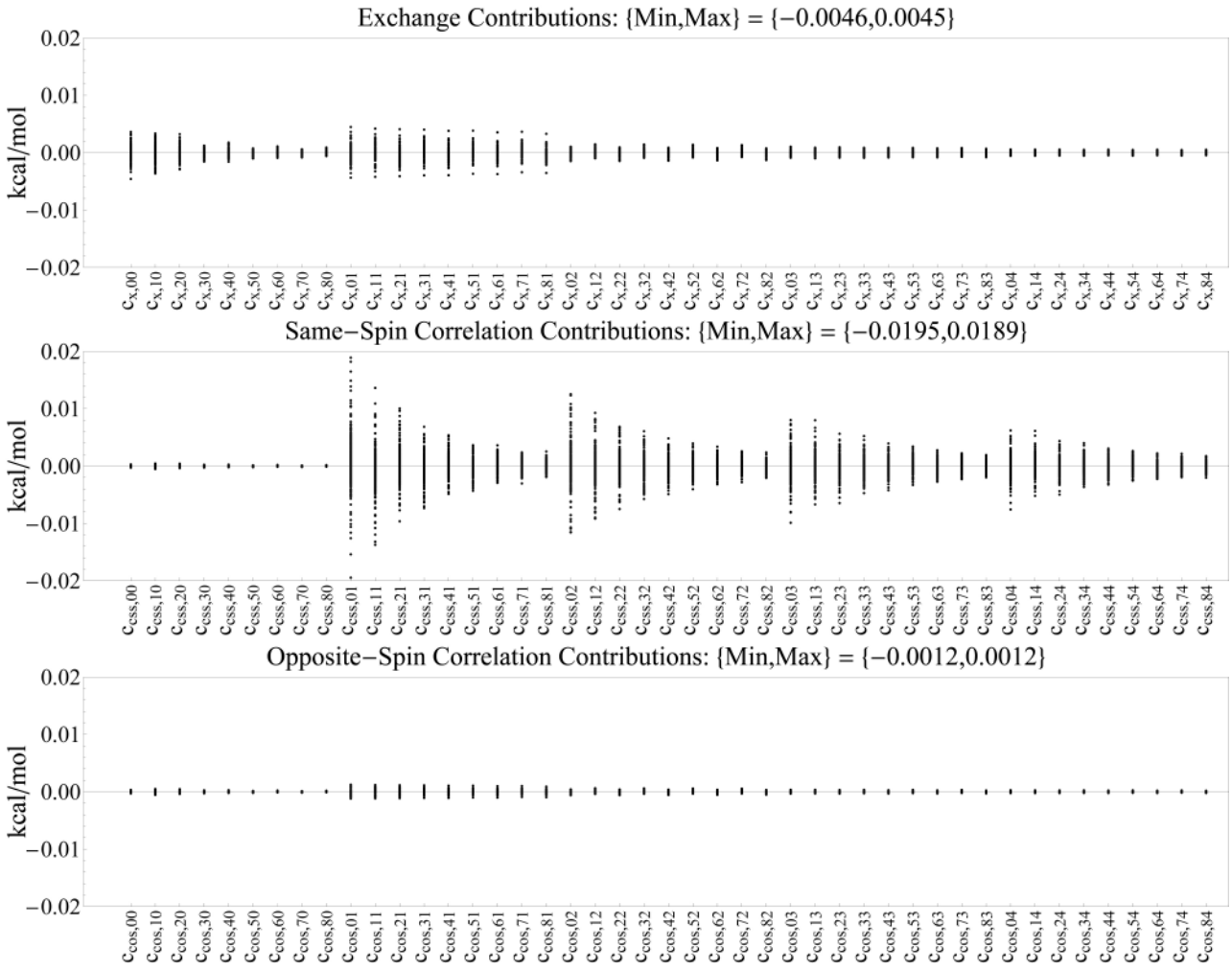

Figure 1: Energetic differences in kcal/mol between the (99,590)/SG-1 data and the (250,590)/SG-1 data for each of the 135 contributions for all 2248 data points in the training and primary test sets.

optional parameters by 3. This truncation reduces the original parameter space from 135 to 72. With 72 selectable parameters, it is possible to expand from 135C5 to 72C7, since 72C7 = 1,473,109,704. Clearly, it is still essential to devise a scheme to allow for the exploration of fits with more than 7 parameters.

From all of the 7-parameter fits resulting from the 72C7 optimization, the top 100,000 (ranked by total RMSD) are analyzed, since the total RMSD is a good indicator of both training set performance (fitting) and primary test set performance (transferability). From these 100,000 fits, those with exchange ICFs that go below zero (resulting in positive exchange contributions) are removed on physical grounds. Since the change in the parameters (Δb) from the least-squares fits can be used to predict energies corresponding to all of the data points (via $E_{LSTSQ} = E_{DFT} + A\Delta b$), the (99,590)/SG-1 and (250,590)/SG-1 data is used to compute 2 sets of energies ($E_{LSTSQ}^{(99,590)}$ and $E_{LSTSQ}^{(250,590)}$) for all of the remaining fits. In order to acquire these energies, E_{DFT}, A, and Δb are taken from the respective grid. The 2 sets of energies are compared and only fits that have a maximum grid-based error of 0.01 kcal/mol across all 2248 data points are kept. The remaining fits are filtered once again, such that those with parameters with a magnitude greater than 30 are removed.

The remaining fits are analyzed in order to determine the coefficient that is most commonly used. This coefficient is then compulsorily selected in the next set of least-squares fits in order to allow for the exploration of 8-parameter fits. This procedure was repeated until a minimum in the total RMSD was found. Since the minimum was found at 15 parameters, 9 coefficients ($c_{x,10}$, $c_{x,01}$, $c_{x,11}$, $c_{x,02}$, $c_{css,10}$, $c_{css,02}$, $c_{css,32}$, $c_{css,42}$, $c_{cos,10}$), which will henceforth be referred to as the "Best 9", had to be compulsorily selected in order to reach the 16-parameter mark at which the total RMSD increased. The progression from the 7-parameter fits to the 16-parameter fits can be tracked in Table 2. In addition, the total RMSDs of the surviving fits are plotted in Figure 2. The 15-parameter fit with the lowest RMSD was self-consistently optimized in order to finalize the parameters. However, after a single self-consistent cycle, it became clear that the least-squares fit RMSDs from the first cycle were inaccurate by more than 0.2 kcal/mol on average, primarily for the thermochemistry datasets.

Table 2: Progression from the 7-parameter fits to the 16-parameter fits based on the LSDA+VV10 data. The first column indicates the additional coefficient that was frozen (compulsorily selected) in order to achieve the associated set of fits. The second column contains the total number of least-squares fits that were performed, of which only the top 100,000 (ranked by total RMSD) were analyzed. The fourth column indicates the number of fits (of 100,000) that remained after the first filtering criterion ($\min(g_x(w_{x,\sigma}, u_{x,\sigma}))\geq 0$) was applied. The fifth column indicates the number of fits from the previous column that remained after the second filtering criterion ($\max(|E_{LSTSQ}^{(99,590)} - E_{LSTSQ}^{(250,590)}|)\leq 0.01$ kcal/mol) was applied. The sixth column indicates the number of fits from the previous column that remained after the third filtering criterion ($\max(|b|)\leq 30$) was applied. Finally, the last 2 columns indicate the coefficient that was most commonly utilized in the surviving fits (shown in Column 6) and the number of times that coefficient appeared.

Frozen	# of Initial Fits	# (Fitted)	g_x	Grid	|b|	Common	# of Remaining Fits
—	1,473,109,704	7	87,506	29,521	29,025	$c_{x,01}$	27,248
$c_{x,01}$	1,329,890,705	8	83,605	45,474	44,828	$c_{x,10}$	44,695
$c_{x,10}$	1,198,774,720	9	55,310	16,572	16,436	$c_{x,02}$	16,155
$c_{x,02}$	1,078,897,248	10	40,900	3,398	3,382	$c_{x,11}$	2,343
$c_{x,11}$	969,443,904	11	17,684	305	290	$c_{css,32}$	224
$c_{css,32}$	869,648,208	12	10,192	90	36	$c_{css,42}$	33
$c_{css,42}$	778,789,440	13	23,664	157	58	$c_{css,10}$	43
$c_{css,10}$	696,190,560	14	3,126	52	42	$c_{css,02}$	41
$c_{css,02}$	621,216,192	15	117	19	16	$c_{cos,10}$	16
$c_{cos,10}$	553,270,671	16	660	62	36	$c_{cos,01}$	33

In order to overcome the issue of inaccurate least-squares fit RMSDs, the contributions were recalculated in the (99,590)/SG-1 grid and (250,590)/SG-1 grid with the "Best 9" parameters fixed. With the updated contributions, all 10-parameter (63C1) through 16-parameter (63C7) fits were recomputed and filtered as before: $\min(g_x(w_{x,\sigma}, u_{x,\sigma}))\geq 0$, $\max(|E_{LSTSQ}^{(99,590)} - E_{LSTSQ}^{(250,590)}|)\leq 0.01$ kcal/mol, and $\max(|b|)\leq 30$.

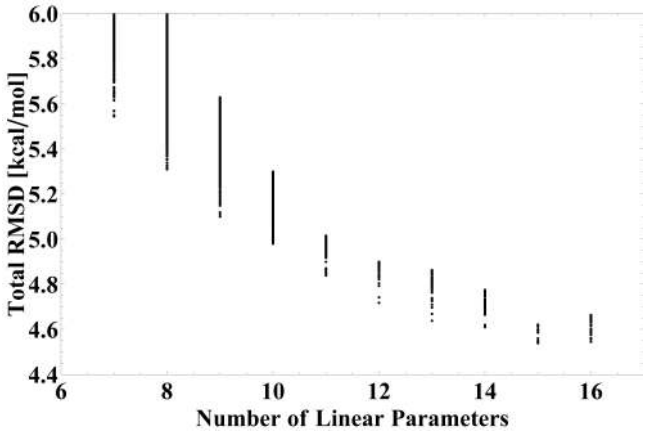

Figure 2: Total RMSDs in kcal/mol of the surviving 7-parameter through 16-parameter fits based on the LSDA+VV10 data. The filtering criteria are described in Section 2.5 and Table 2.

The resulting fits were plotted (on the left in Figure 3) in order to identify the "optimal" fit based on the same methodology that was used in Reference 13. However, in order to ensure that the resulting density functional would be accurate for intermolecular geometries as well, the interpolated minima for 19 of the PECs in the training and primary test sets (7 PECs from NBC10, 5 PECs from BzDC215, 4 PECs from HBC6, along with the 3 rare-gas dimer PECs) were computed and compared to reference values in order to determine mean absolute deviations (MAD) and maximum absolute deviations (MAX) for each fit. Based on this data, fits with an MAD greater than 0.03 Å and an MAX greater than 0.1 Å were discarded in order to produce the plot on the right in Figure 3. The fit that led to the B97M-V density functional is boxed in Figure 3.

The training set and total RMSDs of the unoptimized B97M-V density functional are 66.86 and 88.8 kcal/mol, respectively, while the same values for B97M-V are 5.77 and 4.82 kcal/mol, respectively. Including the initial cycle (Cycle 1) with the unoptimized B97M-V density functional as well as the "Best 9" cycle, the self-consistent optimization of B97M-V required 7 cycles. For the first 2 cycles, the data points in the training *and* primary test sets were evaluated in order to determine the functional form that would be self-consistently optimized. For the later cycles, only the 1095 data points in the training set were required to finalize the parameters. The parameters from the beginning of all 7 cycles are listed in Table 3.

Table 3: Linear parameters from the beginning of all 7 cycles of the self-consistent optimization of B97M-V. The "Best 9" column refers to the freezing of 9 commonly occurring parameters. The nonlinear parameters that were taken from previous studies[19,80,85] are γ_x = 0.004, γ_{css} = 0.2, γ_{cos} = 0.006, b = 6, and C = 0.01.

Parameter	1	Best 9	2	3	4	5	6 (Final)
$c_{x,00}$	1.000	1.000	1.000	1.000	1.000	1.000	1.000
$c_{x,10}$	0.000	0.384	0.417	0.417	0.416	0.416	0.416
$c_{x,01}$	0.000	1.344	1.327	1.310	1.309	1.308	1.308
$c_{x,11}$	0.000	3.073	3.071	3.070	3.070	3.070	3.070
$c_{x,02}$	0.000	1.780	1.804	1.895	1.900	1.901	1.901
$c_{css,00}$	1.000	1.000	1.000	1.000	1.000	1.000	1.000
$c_{css,10}$	0.000	-2.543	-5.857	-5.668	-5.670	-5.667	-5.668
$c_{css,02}$	0.000	-1.470	-1.879	-1.855	-1.856	-1.855	-1.855
$c_{css,32}$	0.000	-20.450	-20.406	-20.477	-20.498	-20.495	-20.497
$c_{css,42}$	0.000	-18.847	-19.739	-20.341	-20.361	-20.364	-20.364
$c_{cos,00}$	1.000	1.000	1.000	1.000	1.000	1.000	1.000
$c_{cos,10}$	0.000	0.425	2.659	2.516	2.538	2.534	2.535
$c_{cos,01}$	0.000	0.000	1.475	1.553	1.574	1.573	1.573
$c_{cos,32}$	0.000	0.000	-6.159	-6.371	-6.427	-6.426	-6.427
$c_{cos,03}$	0.000	0.000	-5.723	-6.203	-6.295	-6.297	-6.298

The final parameters of B97M-V can be found in the last column of Table 3, and Figure 4 shows the exchange, same-spin correlation, and opposite-spin correlation ICF plots for B97M-V. Compared to recent semi-empirical meta-GGA density functionals, the resulting coefficients are very well-behaved. The 2 largest coefficients enhance variables that are fifth and sixth order overall, yet are still around 20 in magnitude. An encouraging but unintended outcome is that all of the exchange coefficients are positive. The resulting ICFs are well-behaved as well, especially the exchange ICF.

Since the resulting functional form of B97M-V is unique and employs terms that are not commonly found in density functionals, it is important to discuss the similarities and differences between B97M-V and existing density functionals. For clarity, the 3 ICFs of B97M-V are given in Equations 28-30. The motivation for using the particular power series expansion shown in Equation 3 came from Becke's B97, B98, and B00 density functionals.[19,20,23] With B97, a systematic optimization was carried out specifically with the GGA variable, u, for exchange,

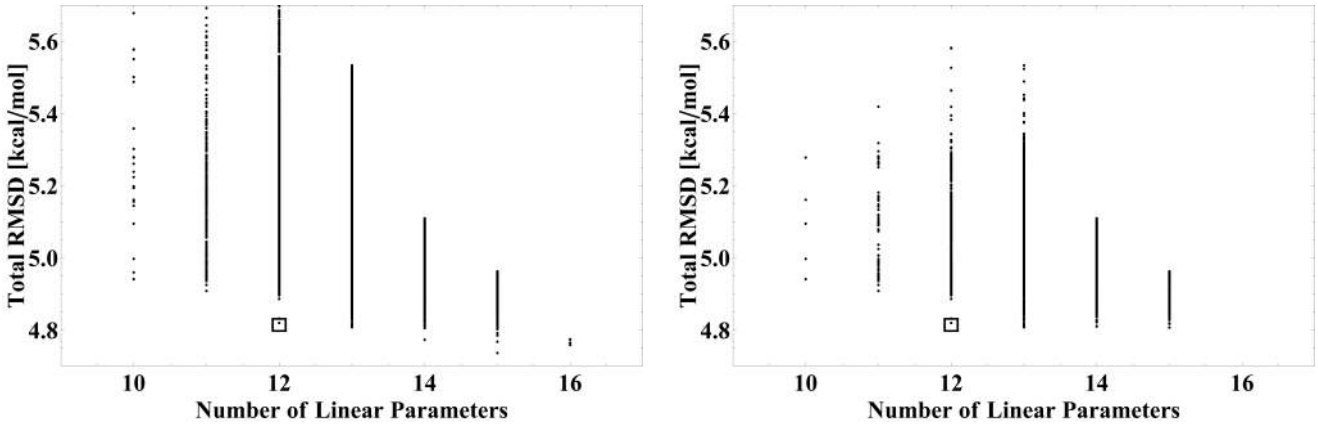

Figure 3: Total RMSDs in kcal/mol of the surviving 10-parameter through 16-parameter fits based on the "Best 9" data. The plot on the left uses the same filtering criteria as Figure 2, while the plot on the right uses 2 additional criteria based on the accuracy of 19 interpolated potential energy curve minima. The fit that led to the B97M-V density functional is boxed.

same-spin correlation, and opposite-spin correlation, while with B98, the same was done with a meta-GGA variable, w', closely related to the w used in this work. The switch from w' to w occurred with the B00 density functional. For B97M-V, the u-dependent ICF of B97 and the w-dependent ICF of B00 were multiplied in order to give Equation 3.

$$g_x(w_{x,\sigma}, u_{x,\sigma}) = 1 + 0.416w_{x,\sigma} + 1.308u_{x,\sigma} + 3.07w_{x,\sigma}u_{x,\sigma} + 1.901u_{x,\sigma}^2 \quad (28)$$

$$g_{css}(w_{c,\sigma\sigma}, u_{c,\sigma\sigma}) = 1 - 5.668w_{c,\sigma\sigma} - 1.855u_{c,\sigma\sigma}^2 - 20.497w_{c,\sigma\sigma}^3u_{c,\sigma\sigma}^2 - 20.364w_{c,\sigma\sigma}^4u_{c,\sigma\sigma}^2 \quad (29)$$

$$g_{cos}(w_{c,\alpha\beta}, u_{c,\alpha\beta}) = 1 + 2.535w_{c,\alpha\beta} + 1.573u_{c,\alpha\beta} - 6.427w_{c,\alpha\beta}^3u_{c,\alpha\beta}^2 - 6.298u_{c,\alpha\beta}^3 \quad (30)$$

In the context of empirical density functionals, the power series, as written in Equation 3, has never been utilized as the starting point for the systematic parameterization of an empirical density functional, particularly for the same-spin and opposite-spin correlation components. The exchange ICFs of the 2005-2011 Minnesota density functionals can be considered as limiting cases of Equation 3, with the u-dependent ICF fixed to the ICFs of either PBE or RPBE (or both), and the w-dependent ICF taking either the B00 form given in Equation 3 or the VSXC form (or both). However, the 2012 meta-nonseparable gradient approximation (NGA) density functionals,[125,126] MN12-L and MN12-SX, use an exchange ICF similar in form to Equation 3, albeit with an additional third power series that is a function of a density-dependent inhomogeneity variable. While the functional forms for the Minnesota density functionals have always been pre-determined (i.e. the parameters that will be optimized are chosen a priori), B97M-V is unique in that the only restrictions on the functional form were placed during the truncation of the parameter space, and the optimization procedure had the freedom to select the parameters that were most conducive to minimizing the total RMSD as well as satisfying the filtering criteria.

The B97M-V correlation functional distinguishes itself even more from existing correlation functionals, because a two-dimensional optimization of a correlation functional has not yet been reported. As far as the Minnesota meta-GGA and meta-NGA density functionals are concerned, the correlation functionals can be divided into 3 distinct classes. The M05 and M05-2X correlation functionals are practically identical to that of B97, with the exception of the SCC factor enhancing the same-spin

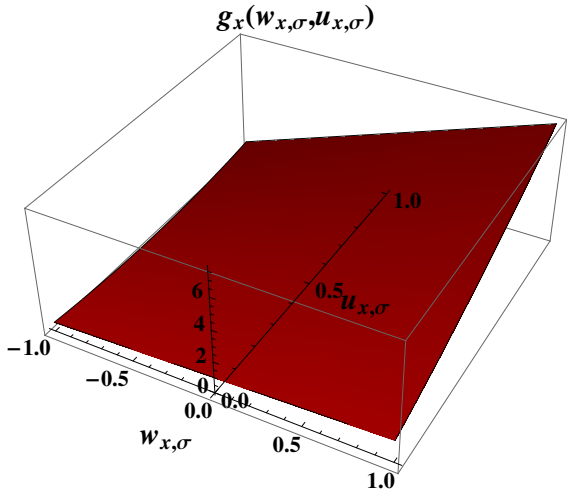

(a)

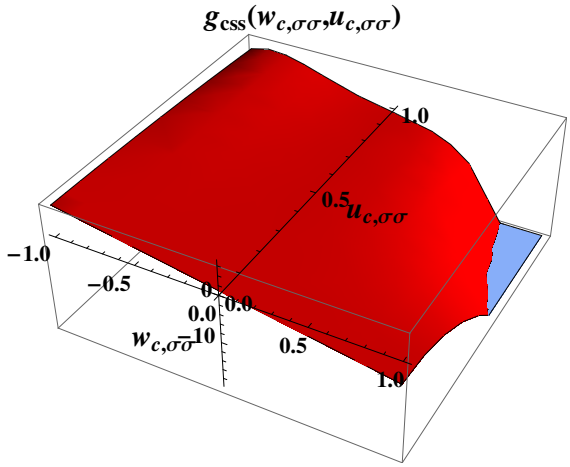

(b)

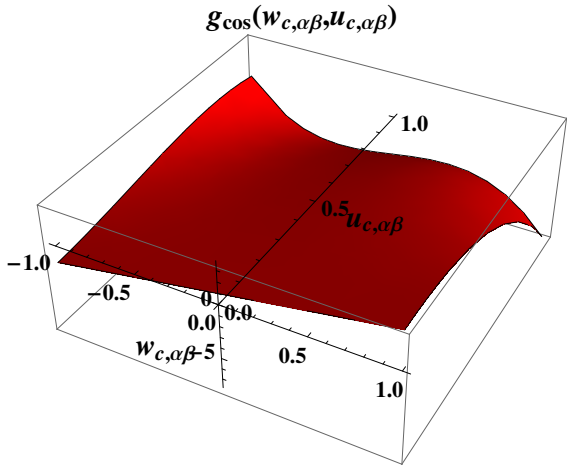

(c)

Figure 4: Exchange, same-spin correlation, and opposite-spin correlation inhomogeneity correction factor plots for the B97M-V density functional.

correlation component. The 2006 Minnesota density functionals inherit the correlation functional of their 2005 counterparts, as well as that of VSXC. Finally, the post-2006 Minnesota meta-GGAs and meta-NGAs no longer partition the correlation energy into same-spin and opposite-spin components, but instead contain 2 w-dependent ICFs that enhance the PW92 correlation energy density per unit volume and the PBE correlation functional gradient correction term.

Taking a closer look at the B97M-V ICF equations, all of the variables that made their way into the exchange ICF can be rationalized. The importance of the first-order terms in w and u is indisputable, and it is thus plausible that the associated second-order cross-term is also helpful. The appearance of the second-order term in u is not surprising either, since this variable is the foundation of the OPTX exchange functional, which was found to be a sound improvement over the B88 exchange functional that contained only the first-order term in u. The same-spin correlation ICF also contains 2 variables (w and u^2) that seem intuitive, as does the opposite-spin correlation ICF (w and u). In fact, the variables that seem most out-of-place are the fifth- and sixth-order variables in the same-spin correlation ICF, and the fifth-order variable in the opposite-spin correlation ICF, since these variables are not ones that can be intuitively selected prior to optimization. Ultimately, the optimization procedure must be credited for shedding light on the importance of these variables.

3 Results and Discussion

3.1 Training Set, Primary Test Set, and Secondary Test Set Performance

To assess the performance of B97M-V, 14 existing density functionals were selected for comparison. These 14 density functionals include 3 local GGA density functionals (PBE-D3, B97-D, VV10), 3 local meta-GGA density functionals (TPSS-D3, M06-L, M11-L), 2 global

hybrid GGA density functionals (B3LYP-D3, B97-D2), 2 global hybrid meta-GGA density functionals (M06, M06-2X), 3 range-separated hybrid GGA density functionals (LC-VV10, ωB97X-D, ωB97X-V), and 1 range-separated hybrid meta-GGA density functional (M11). Table 4 contains information regarding the benchmarked density functionals. Although there is no unique way to count parameters, each density functional in Table 4 is assigned 2 separate numbers regarding its empirical parameter count. The second column lists the total number of linearly independent and nonlinear parameters that were optimized specifically for the given density functional during its development, while the third column lists the total number of linearly independent and nonlinear parameters found in the density functional. As an example, while 12 linear parameters were optimized for B97M-V in this work, 5 additional parameters were borrowed from previous work (γ_x from B86, γ_{css} and γ_{cos} from B97, and b and C from ωB97X-V). Furthermore, parameters that are decided upon prior to optimization, such as s_6 for B97-D and c_x for M06-2X, are only counted in the third column.

Table 4: Details for the 15 density functionals from Table 5. L stands for local, GH stands for global hybrid, RSH stands for range-separated hybrid, DT stands for dispersion tail, and NLC stands for nonlocal correlation. The column labeled "# (Fitted)" lists the number of parameters that were optimized on a training set for the specific density functional, while the column labeled "# (Total)" lists the total number of empirical parameters. c_x refers to the percentage of exact exchange.

Functional	# (Fitted)	# (Total)	c_x	Year	Class	Rung	References
PBE-D3	2	2	0	2010	L GGA w/ DT	2	5,71
B97-D	9	13	0	2006	L GGA w/ DT	2	6
VV10	2	2	0	2010	L GGA w/ NLC	2	5,76,127
TPSS-D3	2	2	0	2010	L MGGA w/ DT	3	36,71
M06-L	34	39	0	2006	L MGGA	3	52
M11-L	44	44	0	2012	L MGGA	3	53
B97M-V	12	17	0	2015	L MGGA w/ NLC	3	Present Work
B3LYP-D3	5	6	20	2010	GH GGA w/ DT	4	9,11,48,71
B97-D2	11	14	19.4	2011	GH GGA w/ DT	4	6,19,123
M06	33	38	27	2008	GH MGGA	4	56
M06-2X	29	34	54	2008	GH MGGA	4	56
LC-VV10	3	3	0-100	2010	RSH GGA w/ NLC	4	5,76
ωB97X-D	15	18	22.2-100	2008	RSH GGA w/ DT	4	128
ωB97X-V	10	13	16.7-100	2014	RSH GGA w/ NLC	4	85
M11	40	40	42.8-100	2011	RSH MGGA	4	59

Table 5 contains the RMSDs for all of the datasets in the training, primary test, and secondary test sets for B97M-V and these 14 existing density functionals. The principal benchmark for success will be how B97M-V compares with other local density functionals: PBE-D3, B97-D, VV10, TPSS-D3, M06-L, and M11-L. However, since hybrid density functionals are usually preferred for higher accuracy DFT calculations, it will be important to see how B97M-V compares with a range of successful hybrids as well.

Before the individual datasets are discussed, the overall performance of the density functionals for thermochemistry (TC) and non-covalent interactions (NC) will be discussed. Of the 15 benchmarked density functionals, M06-2X has the best overall TC performance (3.21 kcal/mol). The next best density functionals for TC are ωB97X-V, ωB97X-D, and B97M-V with RMSDs of 3.6, 3.61, and 3.93 kcal/mol, respectively. It is very encouraging that B97M-V is distinctly the best local density functional for TC, with its closest rivals being B97-D (5.56 kcal/mol) and M06-L (5.63 kcal/mol). This considerable improvement over the best existing local density functionals is a significant gap, and is a validation of the design strategy used to construct B97M-V.

Turning to non-covalent interactions, it is remarkable that B97M-V has the best overall performance (0.22 kcal/mol). After B97M-V, the next best density functionals for non-covalent interactions are ωB97X-V, M06-L, and B97-D2, with RMSDs of 0.32, 0.42 and 0.48 kcal/mol, respectively. The fact that the 2 best density functionals both use the VV10 nonlocal correlation functional is a testament to the accuracy of this approach for treating long-range correlation. Comparing against existing local density functionals, B97M-V is almost 2 times better than the best alternative, M06-L. Furthermore, it is a striking indication of the versatility of the meta-GGA form that B97M-V (0.22 kcal/mol) is more than 30% better than ωB97X-V (0.32 kcal/mol), which was designed by a nearly identical procedure and includes range-separation, though not τ dependence.

Since it would be tedious to individually address the performance of the 15 benchmarked

Table 5: RMSDs in kcal/mol for all of the datasets in the training, primary test, and secondary test sets for B97M-V and 14 existing density functionals. The datasets above the first thick black line are in the training set, the datasets between the first and second thick black lines are in the primary test set, while the datasets between the second and third thick black lines are in the secondary test set. Within the training, primary test, and secondary test sets, datasets above the thin black line contain thermochemistry (TC) data points, while datasets below the thin black line contain non-covalent interactions (NC) data points. The last section of the table contains overall unweighted statistics for TC and NC. The row labeled TC* is TC with AE8 removed. The column labeled "Zero" contains the RMSDs of the energies in each dataset and is meant to give perspective to the magnitudes of the RMSDs in the following columns.

kcal/mol	Zero	PBE-D3	B97-D	VV10	TPSS-D3	M06-L	M11-L	B97M-V	B3LYP-D3	B97-D2	M06	M06-2X	LC-VV10	ωB97X-D	ωB97X-V	M11
HAT707	74.79	7.79	5.62	7.23	6.21	5.86	5.43	3.99	4.27	3.98	4.83	3.63	6.81	4.14	4.28	4.28
BDE99	114.98	8.96	4.58	6.63	4.96	6.14	4.61	3.52	3.91	3.18	3.72	2.99	5.39	3.03	3.38	4.10
TAE_nonMR124	381.05	16.85	5.18	12.46	5.92	5.54	6.62	3.79	5.23	4.06	3.94	3.24	5.30	3.65	3.34	4.37
SN13	25.67	5.56	4.20	3.67	3.71	1.58	3.19	1.39	1.89	0.97	2.03	1.01	2.65	0.96	1.01	2.19
ISOMER20	46.43	4.53	3.83	4.34	4.38	4.11	4.46	3.00	2.30	2.30	2.53	1.47	1.85	1.86	1.64	1.94
DBH24	28.34	10.27	7.18	9.86	9.57	5.38	3.54	4.99	5.23	4.36	2.97	1.12	3.02	2.07	1.81	1.48
EA6	46.12	4.71	2.07	5.28	2.27	2.39	6.17	3.86	3.49	1.45	1.91	1.95	2.10	1.89	2.34	1.33
IP6	260.50	5.07	2.68	7.64	4.65	2.26	3.36	3.91	6.16	3.19	3.23	2.86	5.03	3.01	3.76	5.79
AE8	42810.90	30.54	6.94	64.43	17.97	9.22	15.27	8.12	15.89	2.25	5.52	1.28	29.82	4.67	1.77	9.23
SW49Rel345	1.55	1.45	1.22	1.26	1.24	0.53	0.22	0.12	0.76	0.79	0.60	0.35	0.36	1.01	0.33	0.17
SW49Bind345	29.30	2.24	1.35	2.47	1.63	0.60	1.54	0.17	1.34	0.69	0.72	0.95	0.58	0.98	0.29	0.25
NBC10-2	0.75	0.20	0.08	0.05	0.16	0.15	0.54	0.11	0.13	0.08	0.28	0.11	0.12	0.13	0.09	0.16
BzDC215	2.25	0.37	0.39	0.22	0.35	0.17	0.34	0.18	0.34	0.36	0.25	0.60	0.60	0.41	0.27	0.65
NBC10-1	1.85	0.30	0.20	0.27	0.21	0.26	0.47	0.22	0.29	0.67	0.58	0.43	0.15	0.41	0.23	0.69
HW30	2.34	0.48	0.40	0.43	0.34	0.35	0.48	0.19	0.35	0.35	0.33	0.46	0.30	0.35	0.20	0.38
S22	9.65	0.60	0.54	0.63	0.45	0.43	0.91	0.23	0.50	0.60	0.77	0.47	0.51	0.41	0.23	0.58
EA7	39.24	2.28	3.86	3.57	2.78	6.07	6.44	3.11	3.56	2.55	2.94	1.97	4.19	2.45	2.28	1.08
IP7	252.70	4.28	4.03	4.76	3.71	3.11	2.89	3.67	5.22	3.41	2.93	3.24	5.30	3.26	2.97	4.56
AlkAtom19	1829.31	20.93	10.48	5.85	9.46	8.11	29.35	1.36	5.50	9.28	4.63	5.27	19.04	2.90	0.71	3.94
AlkIsomer11	1.81	1.44	0.33	0.84	1.50	0.95	0.74	0.19	1.56	0.57	0.22	0.15	0.13	1.04	0.67	0.56
AlkIsod14	10.35	2.54	0.57	2.01	3.74	3.86	2.06	0.48	2.75	1.93	1.68	1.65	1.09	2.31	1.80	2.11
HTBH38	15.97	10.32	7.63	9.22	8.71	4.62	1.86	4.48	5.31	5.12	2.21	1.26	1.50	2.57	2.28	1.68
NHTBH38	33.30	10.42	7.12	10.79	10.31	4.79	3.72	5.16	5.81	4.15	2.64	1.69	3.38	1.73	1.64	1.49
SW49Rel6	1.26	1.91	1.65	1.72	1.68	0.80	0.21	0.07	0.86	1.01	0.89	0.42	0.52	1.34	0.37	0.28
SW49Bind6	62.11	3.72	2.50	4.56	2.35	0.57	3.38	0.35	2.35	0.90	0.92	1.61	0.91	0.99	0.36	0.67
HBC6	12.69	1.12	0.77	1.13	0.89	0.36	0.68	0.26	0.77	0.39	0.31	0.59	1.25	0.61	0.39	0.46
NBC10-3	2.52	0.37	0.19	0.17	0.30	0.47	0.83	0.34	0.35	0.54	0.69	0.63	0.06	0.27	0.37	0.80
S22x5	7.00	0.82	0.40	0.59	0.59	0.42	0.94	0.28	0.65	0.71	0.80	0.47	0.48	0.43	0.41	0.55
S66x8	5.57	0.52	0.43	0.50	0.38	0.31	0.83	0.17	0.43	0.35	0.48	0.35	0.34	0.44	0.22	0.42
S66	6.91	0.46	0.52	0.52	0.32	0.36	0.81	0.18	0.43	0.36	0.53	0.29	0.31	0.52	0.18	0.41
NNTT41	0.05	0.06	0.07	0.03	0.04	0.04	0.32	0.01	0.02	0.06	0.12	0.05	0.02	0.15	0.02	0.02
AATT41	0.14	0.05	0.16	0.02	0.09	0.15	0.46	0.03	0.07	0.05	0.23	0.08	0.07	0.21	0.02	0.17
NATT41	0.07	0.06	0.08	0.04	0.04	0.05	0.35	0.01	0.02	0.05	0.13	0.03	0.03	0.15	0.02	0.04
G21EA	40.86	3.97	3.00	4.60	2.74	4.54	6.56	3.41	3.56	1.84	2.46	1.99	3.89	1.98	2.27	2.40
G21IP	265.35	4.81	4.47	5.43	4.77	5.60	4.54	3.64	4.86	3.48	3.78	3.49	5.23	3.82	3.57	4.64
PA8	166.17	1.62	3.70	1.77	3.14	3.36	3.57	3.03	1.28	2.67	2.21	1.98	2.74	2.95	2.20	1.35
Gill12	28.47	7.35	4.84	6.08	5.13	6.71	5.60	5.07	4.09	3.84	3.82	1.78	2.58	3.24	2.32	2.58
A24	2.65	0.41	0.32	0.41	0.23	0.23	0.46	0.17	0.23	0.26	0.25	0.28	0.15	0.15	0.09	0.27
X40	4.94	0.59	0.59	0.63	0.47	0.48	1.23	0.20	0.34	0.43	0.57	0.28	0.41	0.49	0.21	0.54
H2O6Bind8	46.96	4.54	3.84	5.68	2.35	0.99	4.02	0.41	3.07	0.32	1.02	2.23	2.66	1.53	0.68	0.66
HW6F	81.42	2.30	4.49	3.55	0.95	2.32	1.18	0.45	1.79	0.73	1.96	4.77	2.40	1.30	0.21	2.81
HW6Cl	57.71	3.54	3.43	5.08	1.75	1.45	2.92	0.25	1.44	0.48	1.93	3.49	2.67	0.62	0.49	2.10
CYCONF	2.10	0.99	0.56	0.57	0.99	0.39	0.57	0.24	0.29	0.37	0.16	0.30	0.78	0.41	0.11	0.51
DS14	3.70	0.47	0.37	0.52	0.25	0.25	0.59	0.09	0.23	0.25	0.34	0.20	0.12	0.18	0.05	0.30
WATER27	67.48	6.53	2.56	7.07	4.44	1.34	4.60	0.74	3.68	1.42	1.70	3.66	3.35	1.48	1.42	1.62
TC	3836.93	10.10	5.56	9.81	6.45	5.63	6.68	3.93	4.66	3.97	4.18	3.21	6.79	3.61	3.60	3.97
TC*	299.75	9.76	5.55	7.98	6.28	5.59	6.57	3.87	4.45	3.98	4.17	3.22	6.27	3.60	3.61	3.90
NC	14.95	1.23	0.82	1.36	0.85	0.42	1.08	0.22	0.77	0.48	0.57	0.77	0.72	0.54	0.32	0.55
TC Train	4319.60	10.30	5.43	10.44	6.31	5.75	5.64	3.96	4.65	3.83	4.45	3.36	6.86	3.82	3.88	4.23
TC Primary Test	691.59	11.19	6.94	8.02	8.19	5.09	11.41	3.84	4.99	5.09	2.76	2.50	7.60	2.33	1.85	2.30
TC Secondary Test	186.16	4.84	4.06	5.04	4.16	5.30	5.33	3.77	4.13	3.05	3.30	2.74	4.31	3.18	2.92	3.54
NC Train	9.67	0.89	0.64	0.90	0.69	0.33	0.65	0.18	0.56	0.51	0.47	0.54	0.45	0.55	0.25	0.53
NC Primary Test	10.56	0.82	0.60	0.87	0.60	0.35	0.89	0.20	0.58	0.43	0.52	0.44	0.54	0.48	0.27	0.44
NC Secondary Test	37.43	3.13	1.92	3.57	2.04	0.90	2.39	0.38	1.80	0.69	1.02	2.07	1.76	0.85	0.64	1.09

density functionals on the 45 datasets in Table 5, only a handful of datasets will be discussed. TAE_nonMR124 is comprised of the atomization energies of 124 small molecules computed at the Weizmann-4 (W4) level of theory, and is an indicator of performance for computational thermodynamics. B97M-V has an RMSD of 3.79 kcal/mol on this dataset, performing better than 11 of the benchmarked density functionals, and worse than M06-2X (3.24 kcal/mol), ωB97X-V (3.34 kcal/mol), and ωB97X-D (3.65 kcal/mol). After B97M-V, the next best local density functionals for TAE_nonMR124 are B97-D (5.18 kcal/mol) and M06-L (5.54 kcal/mol).

DBH24 is a training dataset that contains 24 forward and reverse barrier heights computed (at least) at the Weizmann-3.2 (W3.2) level of theory, and is an indicator of performance for computational kinetics. The performance of B97M-V for this dataset (4.99 kcal/mol) is poor relative to the best hybrids (M06-2X with an RMSD of 1.12 kcal/mol) due to the absence of exact exchange. Indeed, most of the hybrid density functionals perform considerably better than B97M-V, and this poor performance is a weakness of B97M-V and all local density functionals. Compared to the 6 existing local density functionals considered, B97M-V ranks second (behind M11-L at 3.54 kcal/mol), is comparable to M06-L (5.38 kcal/mol), and is 2 times more accurate than both PBE-D3 and TPSS-D3. Similar results are seen for the barrier height datasets in the primary test set (HTBH38 and NHTBH38), indicating transferability of these conclusions.

Moving on to the non-covalent interactions in the training set, B97M-V has the best performance for both the relative and binding energies of the $SO_4{}^{2-}(H_2O)_n$ ($n = 3-5$) clusters. Compared to density functionals that utilize dispersion tails (DFT-D2 or DFT-D3), B97M-V is 10 times more accurate than PBE-D3 and TPSS-D3 and 5 times more accurate than ωB97X-D for these 2 datasets (SW49Rel345 and SW49Bind345). It even outperforms the range-separated hybrid meta-GGA density functional, M11, which was previously the best performer for both datasets. The S22 dataset by Hobza and coworkers is often used to assess the performance of density functionals for hydrogen-bonded, dispersion-bound, and mixed dimers. The top 2 performers for this dataset are B97M-V and ωB97X-V, both with RMSDs of 0.23 kcal/mol. The next best density functionals are ωB97X-D and M06-L, with RMSDs almost twice as large (0.41 and 0.43 kcal/mol, respectively).

A dataset in the thermochemistry section of the primary test set that is challenging for local and hybrid density functionals alike is AlkAtom19, which contains the atomization energies of 19 alkanes ranging from methane to octane. Surprisingly, B97M-V performs second best (1.36 kcal/mol) out of all 15 density functionals, coming second to ωB97X-V (0.71 kcal/mol). For comparison, M06-2X, which has the best overall thermochemistry performance, has an RMSD of 5.27 kcal/mol for AlkAtom19, while the other Rung 3 density functionals have RMSDs ranging from 8.11 (M06-L) to 29.35 (M11-L) kcal/mol. The performance of B97M-V is also very impressive for 2 datasets derived from the molecules in AlkAtom19: AlkIsomer11 and AlkIsod14. For the isomerization energies, B97M-V (0.19 kcal/mol) performs almost as well as the 2 best density functionals: LC-VV10 (0.13 kcal/mol) and M06-2X (0.15 kcal/mol). In comparison, the RMSD of ωB97X-D is more than 5 times larger, as are the RMSDs of PBE-D3, TPSS-D3, M06-L, and B3LYP-D3. B97M-V has the best performance for the isodesmic reaction energies, with a very small RMSD of 0.48 kcal/mol. The next best density functional is B97-D with an RMSD of 0.57 kcal/mol, followed by LC-VV10 (1.09 kcal/mol). To put the performance of B97M-V in perspective, the range of RMSDs for AlkIsod14 is rather large: 0.48 kcal/mol (B97M-V) to 3.86 kcal/mol (M06-L).

Moving on to the non-covalent interactions in the primary test set, the transferability of the parameters of B97M-V can be checked by considering the relative and binding energies of the $n = 6$ sulfate-water clusters. As intended, B97M-V performs superbly for SW49Rel6 and SW49Bind6, outperforming all of the benchmarked density functionals. Its RMSD for

SW49Rel6 (0.07 kcal/mol) is 3 times smaller than that of the next best density functional (M11-L), while its RMSD for SW49Bind6 (0.35 kcal/mol) is on par with ωB97X-V and 3 times smaller than that of ωB97X-D. The S66 dataset was created by Hobza and coworkers to extend the scope of the S22 dataset to non-covalent interactions that are common in biomolecules. As with S22, the top 2 performers for this dataset are B97M-V and ωB97X-V, both with RMSDs of 0.18 kcal/mol. B97M-V has an RMSD that is 40% less than the value of the next best local meta-GGA density functional, which is TPSS-D3.

The A24 dataset consists of very accurate CCSD(T)/CBS binding energies for small molecules and is a valuable transferability test for B97M-V, since only a few of the interactions that are in A24 were in the training set. Since the binding energies associated with the interactions in A24 are very small, the resulting RMSDs are generally small as well, ranging from 0.09 kcal/mol (ωB97X-V) to 0.46 kcal/mol (M11-L). After ωB97X-V, the next best density functionals are LC-VV10 (0.15 kcal/mol), ωB97X-D (0.15 kcal/mol), and B97M-V (0.17 kcal/mol). Herbert and coworkers recently reported[114] that density functionals such as LC-VV10 and M06-2X perform poorly for halide-water clusters. Specifically, the systems of interest are $F^-(H_2O)_n$ and $Cl^-(H_2O)_n$, for $n = 1 - 6$. ωB97X-V has the best performance for the interactions containing the fluorine anion (0.21 kcal/mol), followed closely by B97M-V (0.45 kcal/mol). Since these binding energies are large, it is important to consider the RMSD range (0.21 kcal/mol for ωB97X-V to 4.77 kcal/mol for M06-2X) in order to comprehend the superb performance of both ωB97X-V and B97M-V. For HW6F, the next best density functionals are B97-D2 (0.73 kcal/mol) and TPSS-D3 (0.95 kcal/mol). On the other hand, for the interactions that contain the chlorine anion, B97M-V has the best performance, with an RMSD of only 0.25 kcal/mol (the largest is VV10 at 5.08 kcal/mol). B97M-V is followed by B97-D2 (0.48 kcal/mol) and ωB97X-V (0.49 kcal/mol), while the best Minnesota density functional is M06-L, with an RMSD of 1.45 kcal/mol.

Finally, the performance of B97M-V and its fellow density functionals can be assessed for water clusters via the H2O6Bind8 (8 binding energies of water hexamers) and WATER27 (23 binding energies of neutral and charged water clusters from dimers to octamers) datasets. B97M-V has the second smallest RMSD for H2O6Bind8 (0.42 kcal/mol) and the smallest RMSD for WATER27 (0.74 kcal/mol), even though the only water cluster in the entire training set was the water dimer in S22. The performance of B97M-V for WATER27 is almost 2 times better than the next best density functional, M06-L (1.34 kcal/mol), and almost 10 times better than VV10 (7.07 kcal/mol).

3.2 Benzene Dimer and Coronene Dimer

The parallel-displaced benzene dimer is a textbook example of π-π stacking and its binding energy has been recently determined to an extremely high level of accuracy (-2.65 ± 0.02 kcal/mol) by Xantheas and coworkers.[129] Using their CCSD(T)/aug-cc-pVTZ optimized dimer geometry and the (99,590)/SG-1 grid, binding energies were computed for all 15 benchmarked density functionals in the aTZ and aQZ basis sets. In addition, aug-cc-pV5Z (a5Z) binding energies were computed for the Rung 2 and 3 density functionals. With these results, summarized in Table 6, the density functionals can be assessed with respect to accuracy, as well as their basis set convergence.

Considering the basis set limit (BSL) values, 8 of the 15 density functionals (PBE-D3, B97-D, VV10, TPSS-D3, B97M-V, B3LYP-D3, LC-VV10, and ωB97X-V) predict the binding energy to within 0.20 kcal/mol of the -2.65 kcal/mol target. All 5 Minnesota density functionals underbind the dimer by between 0.3 kcal/mol (M06-2X) and 1.3 kcal/mol (M11), while ωB97X-D overbinds by almost 0.5 kcal/mol. The basis set convergence of B97M-V is very satisfactory, as the aQZ result is equivalent to the a5Z result, and both differ from the aTZ value by only 0.07 kcal/mol. These results suggest that for weak intermolecular in-

teractions, B97M-V is almost fully converged at the aTZ basis set level, and is fully converged at the aQZ basis set level. Most of the other density functionals also converge satisfactorily with basis set, although consistent with trends reported recently,[130] all of the Minnesota density functionals except M06-2X have unusually large differences between the aTZ basis set value and the largest basis set value (reported as Δ values in Table 6).

Table 6: Equilibrium binding energies in kcal/mol for the parallel-displaced benzene dimer in 3 different basis sets: aug-cc-pVTZ (aTZ), aug-cc-pVQZ (aQZ), and aug-cc-pV5Z (a5Z). Binding energies in the a5Z basis set were only computed for density functionals without exact exchange. The last column contains the difference in binding energy between the aTZ basis set value and the largest basis set value (a5Z for Rungs 2 and 3; aQZ for Rung 4). The (99,590)/SG-1 grid was used for all density functionals. The CCSD(T)/CBS binding energy for the parallel-displaced benzene dimer is -2.65 ± 0.02 kcal/mol, as determined by Xantheas and coworkers.[129]

kcal/mol	aTZ	aQZ	a5Z	Δ
PBE-D3	-2.70	-2.62	-2.55	-0.16
B97-D	-2.71	-2.59	-2.54	-0.17
VV10	-3.08	-2.90	-2.85	-0.23
TPSS-D3	-2.72	-2.62	-2.59	-0.13
M06-L	-2.71	-2.11	-2.23	-0.49
M11-L	-2.91	-1.78	-1.95	-0.96
B97M-V	-2.80	-2.73	-2.73	-0.07
B3LYP-D3	-2.60	-2.48	-	-0.11
B97-D2	-1.90	-1.83	-	-0.08
M06	-2.32	-1.87	-	-0.45
M06-2X	-2.53	-2.37	-	-0.16
LC-VV10	-2.83	-2.69	-	-0.14
ωB97X-D	-3.29	-3.12	-	-0.17
ωB97X-V	-2.80	-2.69	-	-0.12
M11	-2.08	-1.39	-	-0.68

In order to explore whether B97M-V can be successfully applied to larger interactions, the binding energy of the parallel-displaced coronene dimer,[131–133] a dispersion-bound system that is nearly 4 times larger than the benzene dimer, was examined. The calculations were performed in the aTZ basis set with the (99,590)/SG-1 grid. While there is no definitive reference value for the binding energy of the parallel-displaced coronene dimer, 2 recent attempts[131,133] at determining a complete basis set (CBS) value resulted in counterpoise-corrected binding energies of $E_{bind,1}^{CBS}$ = -19.98 kcal/mol and $E_{bind,2}^{CBS}$ = -24.36 kcal/mol. The first reference value was arrived at via the following equation:

$$E_{bind,1}^{CBS} = E_{QCISD(T)}^{aDZ^*} + ([E_{MP2}^{aTZ^*}] - [E_{MP2}^{aDZ^*}]) \quad (31)$$

$$E_{bind,1}^{CBS} = -17.674 + ([-34.610] - [-32.303]) = -19.981 \quad (32)$$

with the asterisk indicating that the cc-pVNZ basis was used for hydrogen and the cc-pVNZ and aug-cc-pVNZ basis sets were alternated for the carbon atoms. The second reference value was arrived at via the following equation:

$$E_{bind,2}^{CBS} = E_{MP2}^{CBS^*} + ([E_{QCISD(T)}^{aDZ^*}] - [E_{MP2}^{aDZ^*}]) \quad (33)$$

$$E_{bind,2}^{CBS} = -38.984 + ([-17.674] - [-32.303]) = -24.355 \quad (34)$$

where $E_{MP2}^{CBS^*} = 1.02(E_{MP2}^{(DT)Z})$ and (DT)Z indicates a two-point extrapolation in the cc-pVDZ and cc-pVTZ basis sets (different extrapolations were used for the HF energy and the MP2 correlation energy). Since it is straightforward to calculate a more accurate estimate of E_{MP2}^{CBS} via $E_{MP2}^{CBS} = E_{HF}^{aQZ} + E_{MP2}^{a(TQ)Z}$, a better MP2 CBS value, E_{MP2}^{CBS} = -38.075 kcal/mol, can be acquired. Using this updated, counterpoise-corrected MP2 CBS value with the QCISD(T) correction yields an updated reference value of $E_{bind,3}^{CBS}$ = -23.45 kcal/mol:

$$E_{bind,3}^{CBS} = E_{MP2}^{CBS} + ([E_{QCISD(T)}^{aDZ^*}] - [E_{MP2}^{aDZ^*}]) \quad (35)$$

$$E_{bind,3}^{CBS} = -38.075 + ([-17.674] - [-32.303]) = -23.446 \quad (36)$$

Simply averaging the 3 CBS estimates results in $E_{bind,avg}^{CBS}$ = -22.59 kcal/mol. Thus, it is safe to assume that the binding energy of the parallel-displaced coronene dimer is in the vicinity of

-22.59 kcal/mol. The binding energy of B97M-V is -22.46 kcal/mol, which is strikingly close to the ωB97X-V value of -22.4 kcal/mol. All 5 of the Minnesota density functionals underbind the dimer, along with B97-D2, PBE-D3, and to a lesser extent, TPSS-D3 and B3LYP-D3. Along with B97M-V and ωB97X-V, the binding energies of B97-D, VV10, and LC-VV10 lie within 1 kcal/mol of $E_{bind,avg}^{CBS}$, while ωB97X-D is the only density functional that overbinds the dimer. As a note, the binding energies of the hybrid density functionals were computed with the PARI-K algorithm of Manzer and Head-Gordon.[134] In order to test the accuracy of the approximation, B3LYP-D3 binding energies were computed with and without the approximation, and the error due to the approximation was found to be around 0.05 kcal/mol.

Table 7: Binding energies in kcal/mol for the parallel-displaced coronene dimer. The binding energies were computed in the aug-cc-pVTZ basis set (2760 basis functions for the dimer) with the (99,590)/SG-1 grid.

kcal/mol	$(C_{24}H_{12})_2$
PBE-D3	-17.33
B97-D	-22.49
VV10	-22.23
TPSS-D3	-19.23
M06-L	-18.04
M11-L	-17.90
B97M-V	-22.46
B3LYP-D3	-20.16
B97-D2	-15.08
M06	-14.62
M06-2X	-17.58
LC-VV10	-23.29
ωB97X-D	-24.35
ωB97X-V	-22.40
M11	-15.75

3.3 $(H_2O)_{20}$ Binding Energies and $(H_2O)_{16}$ Relative Energies

While the WATER27 dataset in Grimme's GMTKN30[108,135,136] database contains 27 data points, the 4 isomers of $(H_2O)_{20}$ were removed from the secondary test set due to their size. Recently, Anacker and Friedrich[137] have updated the reference values[117,138] for these 4 clusters: dodecahedron (-198.6 kcal/mol), edge sharing (-209.7 kcal/mol), fused cubes (-208 kcal/mol), and face sharing (-208 kcal/mol). As a reminder, with the exception of the water dimer in the S22, S22x5, S66, S66x8, A24, and DS14 datasets, water clusters have appeared only in the secondary test set via the H2O6Bind8 and WATER27 datasets, with the largest cluster containing 8 water molecules (WATER27).

The binding energies for the 4 isomers were computed in the aTZ basis set with the (99,590)/SG-1 grid and are shown in Table 8. B97M-V performs remarkably well with respect to the reference binding energies of the water 20-mers, with an RMSD of 0.77 kcal/mol for 4 interactions that have an average binding energy of more than 200 kcal/mol. The next best density functional (B97-D2) is more than 3 times worse, with an RMSD of 2.51 kcal/mol. After B97M-V, the next best local density functional is M06-L, with an RMSD that is more than 5 times larger than that of B97M-V. The 45-fold improvement of B97M-V over VV10 is surprisingly large, as is its 5-fold improvement over ωB97X-V. Interestingly, while most of the density functionals tend to overbind the isomers, the large errors of B97-D and M11-L are actually due to severe underbinding.

Thus far, B97M-V and the 14 existing density functionals have been thoroughly tested for the accurate prediction of the binding energies of large water clusters. In order to test the performance of these density functionals on the relative energetics of water clusters, the relative energies of 5 isomers of $(H_2O)_{16}$ will be evaluated in the aTZ basis set with the (99,590)/SG-1 grid against reference values[139] computed at the CCSD(T)/aTZ level of theory.

In Table 9, the relative energies in the second through sixth columns are computed with respect to the minimum as predicted by the associated method. However, the RMSDs reported in the last column are taken over the relative energies between all 10 unique pairs

Table 8: Binding energies and RMSDs in kcal/mol for 4 isomers of $(H_2O)_{20}$. The binding energies were computed in the aug-cc-pVTZ basis set (1840 basis functions) with the (99,590)/SG-1 grid. The 4 isomers are dodecahedron (dod), edge sharing (es), fused cubes (fc), and face sharing (fs).

kcal/mol	dod	es	fc	fs	RMSD
Reference	-198.60	-209.70	-208.00	-208.00	0.00
PBE-D3	-229.70	-238.86	-235.53	-236.61	29.13
B97-D	-189.80	-197.51	-194.71	-195.18	11.91
VV10	-233.93	-244.95	-242.23	-242.69	34.88
TPSS-D3	-218.93	-227.31	-223.54	-224.87	17.67
M06-L	-191.35	-207.63	-210.01	-206.55	3.97
M11-L	-169.20	-185.68	-187.07	-184.76	24.59
B97M-V	-198.46	-210.10	-209.32	-208.66	0.77
B3LYP-D3	-216.15	-227.70	-225.93	-226.08	17.89
B97-D2	-202.88	-211.53	-209.02	-209.61	2.51
M06	-188.27	-206.69	-211.90	-205.54	5.85
M06-2X	-202.47	-216.59	-218.36	-215.74	7.58
LC-VV10	-208.81	-219.07	-216.49	-217.01	9.29
ωB97X-D	-204.23	-215.63	-214.03	-213.60	5.80
ωB97X-V	-203.39	-214.08	-212.10	-212.37	4.42
M11	-193.59	-206.29	-207.43	-205.01	3.39

Table 9: Relative energies and RMSDs in kcal/mol for 5 isomers of $(H_2O)_{16}$. The relative energies were computed in the aug-cc-pVTZ basis set (1472 basis functions) with the (99,590)/SG-1 grid and are taken with respect to the minimum as predicted by the associated method. The RMSDs are taken over the relative energies between all 10 unique pairs that can be constructed from the 5 isomers.

kcal/mol	4444-a	4444-b	antiboat	boat-a	boat-b	RMSD
Reference	0.00	0.54	0.51	0.25	0.42	0.00
PBE-D3	1.50	1.85	0.49	0.00	0.25	1.21
B97-D	1.45	1.87	0.77	0.00	0.21	1.17
VV10	0.73	1.07	0.58	0.00	0.24	0.61
TPSS-D3	1.89	2.22	0.36	0.00	0.23	1.54
M06-L	0.00	0.37	3.89	3.52	3.60	2.61
M11-L	0.00	0.49	2.19	2.06	2.17	1.37
B97M-V	0.00	0.58	1.16	0.77	0.90	0.42
B3LYP-D3	0.00	0.51	0.24	0.06	0.26	0.16
B97-D2	1.03	1.55	0.55	0.00	0.18	0.92
M06	0.00	0.31	6.37	5.92	5.97	4.51
M06-2X	0.00	0.25	3.71	2.99	3.11	2.36
LC-VV10	0.60	0.86	0.44	0.00	0.17	0.53
ωB97X-D	0.00	0.35	0.54	0.30	0.45	0.14
ωB97X-V	0.22	0.75	0.33	0.00	0.16	0.35
M11	0.00	0.33	3.13	2.55	2.66	1.94

that can be constructed from the 5 isomers. The RMSD range for the 15 benchmarked density functionals is very diverse, with values as low as 0.14 kcal/mol (ωB97X-D) and values as high as 4.51 kcal/mol (M06). In perspective, the performance of B97M-V (0.42 kcal/mol) is promising, as it is the best local density functional. While VV10 drastically overestimated the $(H_2O)_{20}$ binding energies, it performs comparatively well for these relative energies, with an RMSD (0.61 kcal/mol) only slightly worse than that of B97M-V. Other local density functionals, particularly M06-L (RMSD of 2.61 kcal/mol), are significantly worse.

3.4 Additional Energetic Tests

Four sets of additional energetic tests were conducted in order to further assess the transferability of the B97M-V density functional: the HB15, HSG, NC15, and Shields38 datasets. In addition, the potential energy curve of the benzene-argon dimer (a system from the BzDC215 dataset that was not included in the training set) was computed in order to assure that B97M-V maintains the accuracy of VV10 and LC-VV10 in the asymptotic regime. These calculations were carried out in the aTZ basis set with the (99,590)/SG-1 grid. However, due to the delicate nature of the benzene-argon dimer interaction, the (250,590)/SG-1 grid was used instead.

The HB15 dataset[140] is comprised of the equilibrium structures of 15 hydrogen-bonded dimers featuring ionic groups common in biomolecules (acetate, methylammonium, guanidinium, and imidazolium) interacting with neutral donors and acceptors (methanol, water, methylamine, and formaldehyde). The RMSDs of the 15 benchmarked density functionals for this dataset range from 0.23 kcal/mol (B97M-V) to 1.17 kcal/mol (PBE-D3). After B97M-V, the next best performer is ωB97X-V (0.31 kcal/mol), followed by all of the Minnesota density functionals (with RMSDs between 0.41 and 0.54 kcal/mol) besides M11-L (1.03 kcal/mol). The excellent performance of B97M-V further indicates that it can be applied to interactions that were not necessarily included in the training and test sets.

The HSG dataset[141] was developed in order to assess the accuracy with which density functionals and force fields predict the binding

affinities of small ligands to protein receptors. A model protein-ligand complex was selected and decomposed into 21 interacting fragment pairs, and the associated binding energies were evaluated at a high level of theory (and later improved by Sherrill and coworkers[94]). Based on these updated (HSG-A) reference values, the density functional with the best performance is B97M-V, with an RMSD of only 0.14 kcal/mol, followed closely by ωB97X-V, with an RMSD of 0.16 kcal/mol. The best Minnesota density functional is M06-L, with an RMSD that is 3 times larger than that of B97M-V, while the density functional with the worst performance, M11-L, has and RMSD that is 7 times larger than that of B97M-V.

The NC15 dataset[142] comes from a recent study on the basis set convergence of the post-CCSD(T) contribution to weakly-interacting systems. The original study included 21 small dimers, but the LiH dimer has been dropped for this assessment, along with the 5 duplicates from A24. The reference values that are used are the CCSD(T)/CBS ones from Table SI in the Supporting Information of Reference 142. Since the systems in NC15 are very small, the RMSDs for the benchmarked density functionals are correspondingly small, ranging from 0.06 kcal/mol (LC-VV10) to 0.47 kcal/mol (M11-L). B97M-V performs very comparably to LC-VV10, with an RMSD of 0.08 kcal/mol, while the next best local density functional is TPSS-D3 with an RMSD more than twice that of B97M-V. The poor performance of B97-D is surprising and mostly due to its severe overbinding of the He-LiH dimer. The same overbinding issue affects B97-D2, indicating that the culprit might be the DFT-D2 dispersion tail.

The Shields38 dataset[143] includes the binding energies of 38 water clusters ranging from dimers to 10-mers. Since the WATER27 dataset in the secondary test set only contains 10 neutral $(H_2O)_n$ $n = 2-8$ water clusters and the H2O6Bind8 dataset in the secondary test set only contains 8 $(H_2O)_6$ clusters, it was deemed necessary to further assess B97M-V on medium- to large-sized water clusters, due to the unimpressive performance of ωB97X-V for the water 20-mers in Section 3.3. Consistently, the performance of B97M-V is the best observed for the Shields38 dataset as well, further confirming that it is well-suited for applications involving large water clusters. The RMSD of B97M-V (0.35 kcal/mol) is more than 2 times better than that of the next best density functional, which is M11 (0.72 kcal/mol). VV10 massively overbinds once again, with an RMSD 25 times larger than that of B97M-V, while ωB97X-V is only sixth best. While the best local meta-GGA density functional is B97M-V, the best local GGA density functional (B97-D) has an RMSD that is more than 8.5 times larger than that of B97M-V.

Table 10: RMSDs in kcal/mol for 4 datasets. HB15 contains 15 complexes with strong hydrogen bonds, HSG contains 21 interacting fragment pairs from a protein-ligand complex, NC15 contains 15 small non-covalent complexes, and Shields38 contains 38 water clusters with up to 10 water molecules. The binding energies were computed in the aug-cc-pVTZ basis set with the (99,590)/SG-1 grid.

kcal/mol	HB15	HSG	NC15	Shields38
PBE-D3	1.17	0.44	0.29	7.36
B97-D	1.10	0.68	0.35	3.00
VV10	0.99	0.50	0.22	8.75
TPSS-D3	0.87	0.28	0.18	4.52
M06-L	0.43	0.43	0.20	0.78
M11-L	1.03	0.98	0.47	5.69
B97M-V	0.23	0.14	0.08	0.35
B3LYP-D3	0.81	0.33	0.16	4.47
B97-D2	0.64	0.36	0.33	0.90
M06	0.54	0.49	0.19	0.89
M06-2X	0.41	0.43	0.15	2.80
LC-VV10	0.80	0.22	0.06	2.95
ωB97X-D	0.56	0.37	0.13	1.84
ωB97X-V	0.31	0.16	0.07	1.26
M11	0.41	0.69	0.13	0.72

Finally, the performance of 11 of the 15 density functionals is assessed on the benzene-argon dimer PEC. Figure 5 contains the 11 PECs along with the reference PEC and is divided into 3 separate plots: DFT-D containing density functionals (top), Minnesota den-

sity functionals (middle), and VV10-containing density functionals (bottom). Considering the 3 DFT-D density functionals, all of them predict bond lengths that are about 0.1 Å too long. Furthermore, TPSS-D3 overbinds the dimer by about 10%, ωB97X-D underbinds it by about 5%, while B97-D underbinds it by about 10%.

Moving on to the Minnesota density functionals, only M06 comes close to predicting an accurate bond length. M06-L predicts a bond length that is about 0.1 Å too long, while the rest predict bond lengths that are about 0.1 Å too short. With respect to equilibrium binding energies, M06 underbinds the dimer by about 30%, while M06-2X, M11-L, and M11 overbind by 10-30%. Only M06-L gives an equilibrium binding energy that is close to the reference value. A feature of the M11-L PEC that is very hard to miss is its strange long-range behavior. From 4.4 to 5 Å, it predicts repulsive binding energies for the dimer. An exaggeration of this feature of M11-L can be seen for the methane dimer in Figure 6.

The 3 VV10-containing density functionals have almost perfect bond lengths, but only B97M-V gets the equilibrium binding energy just right. LC-VV10 overbinds by about 10%, while ωB97X-V overbinds by about 20%. In terms of consistency, the VV10-containing density functionals are clearly superior for this system. Their long-range behavior is also noticeably better than the rest of the density functionals.

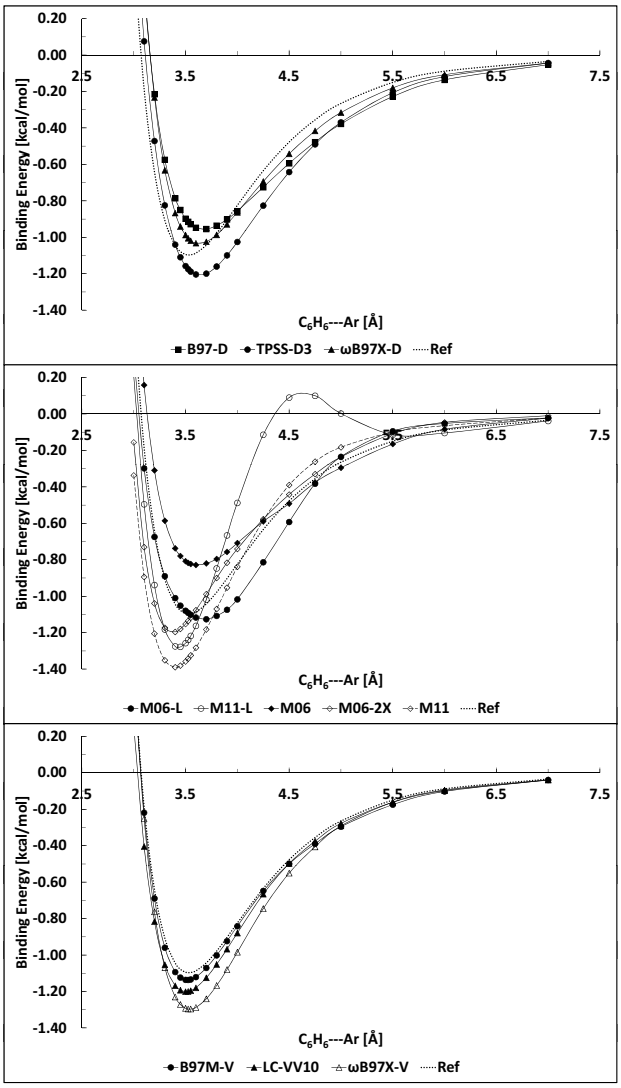

Figure 5: Potential energy curves for the benzene-argon dimer from the BzDC215 dataset computed in the aug-cc-pVTZ basis set with the (250,590)/SG-1 grid.

3.5 Geometries

While the energetics of B97M-V have been thoroughly tested (especially for non-covalent interactions), it is time to move on to tests of intramolecular and intermolecular geometries. The first set of tests are basically free to conduct, since they are based on the interpolated minima of 78 PECs from the training and primary test sets, as well as 10 rare-gas dimer PECs that were additionally computed. In the training set, 3 of the datasets (NBC10-2, BzDC215, and NBC10-1) contain potential energy curves, while in the primary test set, 7 of the datasets (HBC6, NBC10-3, S22x5, S66x8,

NNTT41, AATT41, and NATT41) contain potential energy curves. Five of these 10 datasets were used to generate equilibrium bond length (and binding energy) statistics based on interpolated PEC minima. The PECs in S22x5 did not have enough points near their minima in order to compute reliable values, while the provided points for several of the HBC6 PECs were all post-equilibrium for some density functionals. NBC10-1, NBC10-2, and NBC10-3 have 3, 2, and 2 PECs, respectively, and were combined to recover the NBC10 dataset. For the S66x8 PECs, only the first 5 points (0.9, 0.95, 1, 1.05, and 1.1) were used in the interpolation. Additionally, for each PEC in S66x8, the interpolated minimum was scaled by the closest intermolecular distance of the equilibrium, counterpoise-corrected MP2/TZ optimized structure in order to generate the RMSDs in Table 11. Finally, instead of using data from NNTT41, AATT41, and NATT41 in the primary test set, PECs (1.5 to 15 Å in increments of 0.05 Å) for all 10 rare-gas dimers containing helium, neon, argon, and krypton were computed in the aQZ basis set with the (250,590)/(75,302) grid.

The resulting equilibrium bond length RMSDs are presented in Table 11. The second-to-last column contains the total RMSD for all 88 PECs, while the last column contains the total RMSD for all of the PECs except the rare-gas dimer PECs, for a total of 78. This column was necessary because the rare-gas dimer bond lengths for all of the Minnesota density functionals and ωB97X-D were extremely long and therefore grossly affected the overall RMSD. As a complement to Table 11, Table 12 contains the same statistics for the associated equilibrium binding energies.

The NBC10 dataset contains weakly-bound dimers such as the methane dimer, the benzene-methane dimer, 3 orientations of the benzene dimer, and 2 orientations of the pyridine dimer. The VV10 density functional predicts incredibly accurate bond lengths for these systems, with an RMSD of 0.012 Å. The next best density functional is B97M-V, with an RMSD (0.03 Å) that is still impressive. On the other hand, Table 12 indicates that the equilibrium binding energies of VV10 are 2 times less accurate than those of B97M-V for NBC10. Additional noteworthy performances for the NBC10 bond lengths include B3LYP-D3, LC-VV10, and ωB97X-V, all of which have RMSDs under 0.05 Å. These 3 density functionals have binding energy RMSDs under 0.15 kcal/mol as well, along with B97-D and B97M-V.

The BzDC215 dataset (which is a subset of the true BzDC215 dataset) contains the following PECs: benzene-HF dimer, benzene-water dimer, benzene-ammonia dimer, benzene-methane dimer, and benzene-HCl dimer. For this dataset, the density functionals with the best bond lengths are M06, ωB97X-V, B97M-V, and TPSS-D3, all of which have RMSDs under 0.03 Å. Of these 4 density functionals, B97M-V has the best equilibrium binding energy RMSD (0.21 kcal/mol). The smallest binding energy RMSD is achieved by M06-L (0.17 kcal/mol), but its bond length RMSD of 0.072 Å is 3 times larger than that of B97M-V.

The S66x8 dataset is a diverse collection of 66 dimers, containing electrostatics-dominated interactions, as well as dispersion-dominated interactions. B97M-V gives the most accurate bond lengths for this dataset, with an RMSD of only 0.02 Å, followed by B3LYP-D3 (0.025 Å), VV10 (0.029 Å), and LC-VV10 (0.03 Å). Most of the other density functionals perform reliably, with the exception of B97-D, M11, and M06-2X, all of which have bond length RMSDs in excess of 0.07 Å. With respect to binding energies, the data further confirms that B97M-V and ωB97X-V give the most accurate equilibrium binding energies, with RMSDs of 0.19 and 0.21 kcal/mol, respectively.

As far as the rare-gas dimers are concerned, B97M-V has the smallest bond length RMSD across all 10 dimers, followed by ωB97X-V, VV10, and B3LYP-D3. These 4 density functionals are the only ones with RMSDs smaller than 0.1 Å. Five of the remaining density functionals have RMSDs between 0.1 and 0.2 Å, with the remaining 6 having RMSDs in excess of 0.2 Å: M06-L, M06-2X, ωB97X-D, M06, M11, and M11-L. Given this data, it is straightforward to conclude that systematically-optimized density functionals

that are not tested for transferability during fitting (such as ωB97X-D and the Minnesota density functionals) are more likely to perform poorly for the rare-gas dimers. Besides B97M-V and ωB97X-V (both of which were almost guaranteed to perform well for the rare-gas dimers via the transferability tests), only 2 systematically-optimized density functionals (B97-D and B97-D2) perform reasonably well for the rare-gas dimers, most likely due to the conservative $m = 2$ truncation that was employed for their ICFs.

The overall statistics can identify the best density functionals for these types of interactions. Considering the second-to-last column of both Tables 11 and 12, it is clear that B97M-V has the most accurate bond lengths overall, with an RMSD of 0.028 Å. The next best density functional, VV10, has an RMSD that is 0.01 Å larger, followed by ωB97X-V (0.04 Å) and B3LYP-D3 (0.04 Å). These 4 are the only density functionals that have overall bond length RMSDs under 0.05 Å. With respect to the overall equilibrium binding energies, B97M-V and ωB97X-V are the clear winners, with RMSDs of 0.17 and 0.2 kcal/mol, respectively. The next best density functional (M06-L) has an RMSD of 0.31 kcal/mol, and has an overall bond length RMSD of 0.09 Å (more than 3 times worse than that of B97M-V).

To assess the ability of B97M-V to optimize accurate geometries, 3 sets of geometries were benchmarked in the aug-cc-pVTZ basis set and the results are shown in Table 13. The first set, taken from the work of Tentscher and Arey,[144] contains 18 bond lengths of 18 small radicals. The *ab Initio* Best Estimate bond lengths from the second-to-last column of Table 1 in Reference 144 are taken as the reference in order to generate the MADs shown in Table 13. For this set of geometries, B97M-V and M06-L perform indistinguishably, with bond length MADs of 0.55 pm. The next best density functionals are B3LYP-D3 and B97-D2, with MADs of 0.69 pm, while the worst performers are M11 and M11-L, with MADs of 1.33 and 1.87 pm, respectively. The next set of geometries, taken from Bak et al.,[145] contains 28 bond lengths of 19 small molecules. The CCSD(T)/cc-pCVQZ

Table 11: Equilibrium bond length RMSDs in Å for interpolated potential energy curve (PEC) minima from 5 of the datasets in the training and primary test sets, as well as an additional dataset containing PECs for all 10 rare-gas dimers (computed in the aug-cc-pVQZ basis set with the (250,590)/(75,302) grid) containing helium, neon, argon, and krypton. NBC10 is a combination of the NBC10-1, NBC10-2, and NBC10-3 datasets from the training and primary test sets. The column labeled "All" contains RMSDs for all 4 datasets, while the column labeled "All*" excludes the rare-gas dimer data.

Å	NBC10	BzDC215	S66x8	Rare-gas	All	All*
# of Data Points	7	5	66	10	88	78
PBE-D3	0.094	0.035	0.064	0.163	0.083	0.066
B97-D	0.063	0.073	0.070	0.168	0.086	0.069
VV10	0.012	0.032	0.029	0.084	0.038	0.028
TPSS-D3	0.071	0.028	0.057	0.165	0.077	0.057
M06-L	0.072	0.072	0.040	0.233	0.090	0.046
M11-L	0.817	0.042	0.035	1.532	0.566	0.247
B97M-V	0.030	0.024	0.020	0.058	0.028	0.021
B3LYP-D3	0.039	0.043	0.025	0.089	0.040	0.028
B97-D2	0.094	0.047	0.043	0.140	0.067	0.050
M06	0.258	0.020	0.041	0.500	0.187	0.086
M06-2X	0.105	0.116	0.074	0.243	0.112	0.081
LC-VV10	0.040	0.089	0.030	0.152	0.062	0.037
ωB97X-D	0.051	0.042	0.039	0.399	0.140	0.040
ωB97X-V	0.042	0.022	0.036	0.065	0.040	0.036
M11	0.062	0.123	0.071	0.614	0.219	0.075

Table 12: Equilibrium binding energy RMSDs in kcal/mol for interpolated potential energy curve (PEC) minima from 5 of the datasets in the training and primary test sets, as well as an additional dataset containing PECs for all 10 rare-gas dimers (computed in the aug-cc-pVQZ basis set with the (250,590)/(75,302) grid) containing helium, neon, argon, and krypton. NBC10 is a combination of the NBC10-1, NBC10-2, and NBC10-3 datasets from the training and primary test sets. The column labeled "All" contains RMSDs for all 4 datasets, while the column labeled "All*" excludes the rare-gas dimer data.

kcal/mol	NBC10	BzDC215	S66x8	Rare-gas	All	All*
# of Data Points	7	5	66	10	88	78
PBE-D3	0.24	0.49	0.54	0.11	0.49	0.52
B97-D	0.12	0.55	0.52	0.06	0.47	0.50
VV10	0.25	0.30	0.63	0.04	0.55	0.59
TPSS-D3	0.18	0.44	0.40	0.08	0.37	0.39
M06-L	0.38	0.17	0.33	0.13	0.31	0.33
M11-L	0.46	0.19	0.73	0.19	0.65	0.69
B97M-V	0.12	0.21	0.19	0.03	0.17	0.18
B3LYP-D3	0.13	0.49	0.52	0.05	0.47	0.50
B97-D2	0.42	0.51	0.36	0.09	0.36	0.38
M06	0.60	0.28	0.52	0.12	0.48	0.51
M06-2X	0.52	0.78	0.31	0.11	0.36	0.38
LC-VV10	0.11	0.64	0.40	0.07	0.38	0.41
ωB97X-D	0.38	0.57	0.59	0.08	0.54	0.57
ωB97X-V	0.11	0.36	0.21	0.03	0.20	0.21
M11	0.75	0.80	0.39	0.16	0.45	0.47

bond lengths from the last column of Table II in Reference 145 are taken as the reference in order to generate the MADs shown in Table 13. For this set of geometries, M06-L and B3LYP-D2 (MADs under 0.5 pm) perform very well, followed by B97-D2 and B97M-V (MADs under 0.6 pm). The (99,590)/SG-1 grid was used for both the Arey and Bak datasets.

Moving on to intermolecular geometry optimizations, the A19 dataset includes 19 of the 21 equilibrium geometries from A24. Two dimers (water-methane and methane-ethene) were removed because several density functionals optimized these systems to a different orientation than that of the reference structure. The optimizations for the A19 dataset were carried out with the (150,770)/SG-1 grid and the symmetry of the reference structure was preserved. The metric used to assess the performance of the density functionals is the MAD of 19 RMSDs generated by the Kabsch algorithm[146] (calculated by comparing the reference and final geometries). Of the benchmarked density functionals, ωB97X-V is clearly the best performer, with an MAD of only 1.4 pm, while B97M-V comes in second, with an MAD of 2.35 pm. Following B97M-V, 3 density functionals, B97-D2, B3LYP-D3, and LC-VV10, have MADs between 2.5 pm and 3 pm. The next best local density functional after B97M-V is B97-D, with an MAD (4.92 pm) that is more than twice as large as that of B97M-V. Overall, the performance of B97M-V for both intramolecular and intermolecular geometry optimizations is impressive, since these are features that are not necessarily guaranteed from fitting to energetics.

4 Using B97M-V

4.1 Basis Sets

Even though B97M-V was trained in the aQZ basis set for thermochemistry and the aTZ basis set (without counterpoise corrections) for noncovalent interactions, it is inevitable that it will be used with different basis sets. As a result, this section explains how B97M-V should be

Table 13: MADs in picometers (pm) for the 3 geometry datasets discussed in Section 3.5. For the Arey and Bak datasets, the entries are bond length MADs and the optimizations were carried out in the aug-cc-pVTZ basis set with the (99,590)/SG-1 grid. For the A19 dataset, the optimizations were carried out with the (150,770)/SG-1 grid in the aug-cc-pVTZ basis set and the errors are calculated by using the Kabsch algorithm. The A19 column contains MADs of 19 RMSDs calculated by the Kabsch algorithm.

pm	Arey	Bak	A19
# of Data Points	18	28	19
PBE-D3	1.13	1.01	5.57
B97-D	0.90	0.75	4.92
VV10	1.21	1.06	5.87
M06-L	0.55	0.42	5.58
M11-L	1.87	1.78	5.08
B97M-V	0.55	0.57	2.35
B3LYP-D3	0.69	0.48	2.64
B97-D2	0.69	0.52	2.62
M06	1.10	0.87	5.93
M06-2X	1.20	0.87	5.23
LC-VV10	1.31	1.08	2.93
ωB97X-D	0.90	0.71	3.80
ωB97X-V	0.91	0.69	1.40
M11	1.33	0.96	4.25

used and what basis sets are recommended.

In order to assess the basis set dependence of thermochemical quantities, the data points in the W4-11 dataset were computed in a variety of basis sets with the (99,590)/SG-1 grid: cc-pVDZ (DZ), cc-pVTZ (TZ), cc-pVQZ (QZ), 6-311++G(3df,3pd) (LP), pc-1 (pc1), pc-2 (pc2), pc-3 (pc3), def2-SVP (SVP), def2-TZVP (TZVP), def2-QZVP (QZVP), and aug-cc-pVQZ (aQZ). The goal was to identify basis sets substantially smaller than aQZ that can provide results similar in quality to the aQZ results. The corresponding data is shown in Table 14. The values in the second row correspond to the number of basis functions the given basis set has for propane, while the values in the following row are the total atomization energies (TAE) of propane computed with the given basis set. The W4-11 reference value for the TAE of propane is -1007.91 kcal/mol, while the B97M-V aQZ value is -1007.28 kcal/mol. Considering just the values from the third row of Table 14, it is clear that the DZ, pc1, SVP, and TZVP basis sets are insufficient for the calculation of thermochemical quantities. However, in order to arrive at a more solid conclusion, the RMSDs for the 5 subdatasets in the W4-11 dataset are shown in the fourth through eighth rows of Table 14. In addition, the last 6 rows contain overall statistics for all of W4-11 with respect to both the aQZ values as well as the reference values.

Considering both performance with respect to the aQZ basis set as well as the reference, the following basis sets can be potentially recommended as alternatives to the aQZ basis set for thermochemistry (pending further tests): QZ, LP, pc2, pc3, and QZVP. From these recommended basis sets, the smallest one is pc2, which only has 202 basis functions for propane, while aQZ has 608. Thus, even though B97M-V was trained in the aQZ basis set for thermochemistry, it might be sufficient to use a basis set that is 3 times smaller to arrive at results that are of aQZ quality.

Since the molecules in the W4-11 dataset are relatively small, the 5 promising basis sets from the W4-11 study were applied to larger interactions via the AlkAtom19, AlkIsomer11,

Table 14: RMSDs in kcal/mol computed with the (99,590)/SG-1 grid for the 5 sub-datasets comprising the W4-11 dataset in a variety of basis sets: cc-pVDZ (DZ), cc-pVTZ (TZ), cc-pVQZ (QZ), 6-311++G(3df,3pd) (LP), pc-1 (pc1), pc-2 (pc2), pc-3 (pc3), def2-SVP (SVP), def2-TZVP (TZVP), def2-QZVP (QZVP), and aug-cc-pVQZ (aQZ). The last 6 rows contain statistics for the entire W4-11 dataset with respect to both the basis set limit values (aQZ) as well as the reference values. The second row indicates the number of basis functions (BF) the given basis set has for propane, while the third row contains the total atomization energy (TAE) of propane in kcal/mol. The W4-11 reference value for the TAE of propane is -1007.91 kcal/mol.

kcal/mol	DZ	TZ	QZ	LP	pc1	pc2	pc3	SVP	TZVP	QZVP	aQZ
BF (C_3H_8)	82	202	405	261	82	202	464	82	141	411	608
TAE (C_3H_8)	-1004.83	-1008.49	-1007.78	-1007.82	-1000.09	-1008.61	-1008.09	-1020.79	-1005.43	-1007.73	-1007.28
HAT707	8.75	4.73	4.08	4.08	7.28	4.19	3.85	8.08	4.19	3.94	3.99
BDE99	5.74	3.76	3.57	3.64	5.29	3.56	3.64	5.70	3.70	3.59	3.52
TAE_nonMR124	11.72	4.17	3.74	3.92	10.84	3.42	3.85	7.78	4.11	3.88	3.79
SN13	4.65	1.66	1.47	1.35	3.51	1.41	1.37	3.16	1.56	1.41	1.39
ISOMER20	3.87	3.10	3.07	3.01	3.80	3.07	3.01	4.06	3.26	3.03	3.00
RMSD vs. aQZ	6.86	1.36	0.45	0.80	5.98	0.92	1.07	5.47	1.07	0.96	0.00
RMSD vs. Reference	8.91	4.47	3.92	3.95	7.70	3.94	3.78	7.66	4.07	3.84	3.85
MAD vs. aQZ	4.51	0.98	0.34	0.58	4.26	0.69	0.55	3.87	0.72	0.52	0.00
MAD vs. Reference	6.25	3.38	2.95	2.96	5.77	2.94	2.84	5.72	3.12	2.89	2.90
MSE vs. aQZ	1.33	-0.04	-0.13	-0.32	1.02	-0.27	-0.27	-0.91	-0.05	-0.20	0.00
MSE vs. Reference	0.30	-1.07	-1.16	-1.34	-0.01	-1.30	-1.30	-1.94	-1.08	-1.23	-1.03

and AlkIsod14 datasets. The results (computed with the (75,302)/SG-0 grid) are shown in Table 15. The second row of Table 15 lists the number of basis functions the given basis set has for octane, while the third row contains the TAE of octane (the reference is -2482.64 kcal/mol and the B97M-V aQZ result is -2480.94 kcal/mol). At first glance, all of the basis sets appear to predict a reasonable value for the TAE of octane, with the largest deviation being the aQZ result itself (0.07% error). In fact, in the aQZ basis set, B97M-V slightly underestimates the atomization energies of the larger alkanes in AlkAtom19, with an RMSD of 1.35 kcal/mol and an MSE (mean signed error) of 0.73 kcal/mol. Decreasing the size of the basis set increases the effect of basis set superposition error (BSSE) and leads to slightly more binding, resulting in a 7-fold improvement in the AlkAtom19 RMSD with the pc3 basis set. The isomerization energies are relatively insensitive to the basis set, as are the isodesmic reaction energies. **Based on these results, the cc-pVQZ, 6-311++G(3df,3pd), pc-2, pc-3, and def2-QZVP basis sets can be recommended as alternatives to the aug-cc-pVQZ basis set for thermochemistry.**

Moving on to non-covalent interactions,

Table 15: RMSDs in kcal/mol computed with the (75,302)/SG-0 grid for 3 datasets from the primary test set in a variety of basis sets: cc-pVQZ (QZ), 6-311++G(3df,3pd) (LP), pc-2 (pc2), pc-3 (pc3), def2-QZVP (QZVP), and aug-cc-pVQZ (aQZ). The last 6 rows contain statistics for the entire W4-11 dataset with respect to both the basis set limit values (aQZ) as well as the reference values. The second row indicates the number of basis functions (BF) the given basis set has for octane, while the third row contains the total atomization energy (TAE) of octane in kcal/mol. The AlkAtom19 reference value for the TAE of octane is -2482.64 kcal/mol.

kcal/mol	QZ	LP	pc2	pc3	QZVP	aQZ
BF (C_8H_{18})	980	636	492	1124	996	1468
TAE (C_8H_{18})	-2481.93	-2481.88	-2483.40	-2482.73	-2481.37	-2480.94
AlkAtom19	0.60	0.61	0.67	0.19	0.99	1.35
AlkIsomer11	0.21	0.20	0.11	0.30	0.27	0.21
AlkIsod14	0.54	0.43	0.39	0.64	0.62	0.51
RMSD vs. aQZ	0.50	0.50	1.31	0.86	0.28	0.00
RMSD vs. Reference	0.51	0.48	0.49	0.41	0.75	0.94
MAD vs. aQZ	0.33	0.35	0.88	0.60	0.22	0.00
MAD vs. Reference	0.42	0.38	0.42	0.30	0.60	0.73
MSE vs. aQZ	-0.31	-0.35	-0.88	-0.48	-0.13	0.00
MSE vs. Reference	0.42	0.38	-0.16	0.25	0.60	0.73

the A24 dataset was used as an initial test of the basis set convergence of small molecules. The calculations were performed with the (99,590)/SG-1 grid and a total of 25 basis sets were assessed: cc-pVNZ for N={D,T,Q,5} (NZ), aug-cc-pVNZ for N={D,T,Q,5} (aNZ), pc-N for N={0,1,2,3,4} (pcN), aug-pc-N for N={0,1,2,3,4} (apcN), def2-NVP for N={S,TZ,QZ} (NVP), def2-NVPD for N={S,TZ,QZ} (NVPD), and 6-311++G(3df,3pd) (LP). The results are summarized in Table 16. For each basis set, 2 types of statistics with respect to the reference values are reported: root-mean-square deviations (RMSD) and mean signed errors (MSE). Furthermore, the results are presented both with counterpoise corrections (CP), without counterpoise corrections (noCP), as well as their average (AVG=(CP+noCP)/2). Since B97M-V was trained at the noCP aTZ basis set level, the corresponding RMSD of 0.17 kcal/mol is a useful guide for assessing the performance of B97M-V in the remaining 24 basis sets. Immediately, it is clear that the pc0 and apc0 basis sets are incompatible with B97M-V, both with and without counterpoise corrections. In addition, the DZ, pc1, and SVP basis sets have RMSDs greater than 0.25 kcal/mol with counterpoise corrections, and are unacceptable without counterpoise corrections. Basis sets that perform well both with and without counterpoise corrections include 5Z, aTZ, aQZ, a5Z, pc3, pc4, apc2, apc3, apc4, TZVPD, QZVP, QZVPD, and LP, while basis sets that perform well only with counterpoise corrections include TZ, QZ, aDZ, pc2, apc1, SVPD, and TZVP.

For comparison to B97M-V, the last row of Table 16 contains data corresponding to the M06-L density functional computed in the aTZ basis set. While the RMSD of B97M-V improves very slightly from 0.17 kcal/mol to 0.15 kcal/mol when going from noCP aTZ to CP aTZ, the reverse happens for M06-L: the RMSD increases from 0.23 kcal/mol to 0.41 kcal/mol. The fact that the CP and noCP a5Z RMSDs of B97M-V closely match the CP and noCP aTZ RMSDs indicates that for intermolecular interactions involving small molecules, the aTZ basis set can be considered close to the basis set limit for B97M-V. However, since the largest dimer in the A24 dataset is the ethene dimer (the number of basis functions for each basis set is listed in the second column of Table 16), the promising basis sets that were smaller than or equivalent to aTZ were applied to larger intermolecular interactions via the S22 and S66 datasets.

The S22 data (Table 17) looks significantly different from the A24 data. As a reminder, the S22 dataset was included in the training set of B97M-V with a weight of 100. The noCP aTZ RMSD of 0.23 kcal/mol is the smallest RMSD possible, while the pc2, TZVPD, and aQZ basis sets look promising without counterpoise corrections, presenting a degradation of 20% at most compared with the noCP aTZ RMSD. However, the CP aTZ RMSD of 0.33 kcal/mol presents a degradation of 0.1 kcal/mol (40%) from the noCP aTZ result. Considering the aQZ basis set results, it is clear that the noCP and CP results have not converged, indicating that it is much more difficult to converge the binding energies of larger interactions. Additionally, since the interactions in S22 were heavily emphasized in training the parameters of B97M-V, it is possible that going to a larger basis set is leading to underbinding. Considering the CP MSE and noCP MSE values for aTZ and aQZ provides confirmation of this effect. Based on the S22 data, only the TZVPD basis set (to be used without counterpoise corrections) can be recommended as an alternative to noCP aTZ for non-covalent interactions.

For comparison to B97M-V, the last row of Table 17 contains data corresponding to the M06-L density functional computed in the aTZ basis set. While the RMSD of B97M-V degrades by 40% when going from noCP aTZ to CP aTZ, the RMSD of M06-L worsens by more than a factor of 2.5.

Since the S22 dataset was in the training set, it is important to test a dataset of larger interactions from one of the test sets in order to assure that the effect seen with the S22 data is less pronounced for datasets that were not included in the training set. Accordingly, the results for the S66 dataset are provided in Table 18. The S66 data is much more reasonable,

Table 16: RMSDs and MSEs in kcal/mol for the A24 dataset computed in 25 basis sets. The abbreviations are explained in Section 4.1. The second column contains the number of basis functions (BF) for the largest interaction in A24: the ethene dimer. The interactions were computed with the (99,590)/SG-1 grid with counterpoise corrections (CP), without counterpoise corrections (noCP), as well as their average (AVG). The last row contains data for the M06-L density functional in the aTZ basis set for comparison to the B97M-V results.

kcal/mol	BF	CP RMSD	noCP RMSD	AVG RMSD	CP MSE	noCP MSE	AVG MSE
DZ	96	0.29	1.27	0.63	0.16	-0.86	-0.35
TZ	232	0.19	0.65	0.36	0.03	-0.42	-0.19
QZ	460	0.17	0.34	0.22	0.02	-0.20	-0.09
5Z	804	0.15	0.17	0.16	0.01	-0.04	-0.02
aDZ	164	0.16	0.29	0.19	0.03	-0.21	-0.09
aTZ	368	0.15	0.17	0.16	-0.01	-0.05	-0.03
aQZ	688	0.15	0.15	0.15	0.00	-0.03	-0.01
a5Z	1148	0.15	0.15	0.15	0.00	-0.01	0.00
pc0	52	0.95	3.75	2.30	-0.32	-2.45	-1.38
pc1	96	0.25	0.87	0.51	0.00	-0.56	-0.28
pc2	232	0.17	0.28	0.22	0.00	-0.13	-0.06
pc3	528	0.15	0.15	0.15	0.00	-0.01	0.00
pc4	940	0.15	0.15	0.15	0.01	0.00	0.00
apc0	76	1.00	1.96	1.44	-0.43	-1.39	-0.91
apc1	164	0.17	0.49	0.26	0.06	-0.41	-0.18
apc2	368	0.15	0.18	0.16	0.00	-0.09	-0.04
apc3	756	0.15	0.15	0.15	0.00	-0.02	-0.01
apc4	1284	0.15	0.15	0.15	0.00	0.00	0.00
SVP	96	0.26	1.26	0.67	0.10	-0.90	-0.40
SVPD	144	0.16	0.52	0.28	0.02	-0.47	-0.23
TZVP	172	0.21	0.41	0.30	-0.03	-0.22	-0.13
TZVPD	220	0.15	0.15	0.15	0.00	-0.06	-0.03
QZVP	468	0.15	0.18	0.16	0.01	-0.05	-0.02
QZVPD	516	0.15	0.15	0.15	0.00	-0.01	0.00
LP	300	0.15	0.24	0.19	0.01	-0.11	-0.05
aTZ*	368	0.41	0.23	0.31	0.37	0.15	0.26

Table 17: RMSDs and MSEs in kcal/mol for the S22 dataset computed in 15 basis sets. The abbreviations are explained in Section 4.1. The second column contains the number of basis functions (BF) for the largest interaction in S22: the adenine-thymine complex. The interactions were computed with the (75,302)/SG-0 grid with counterpoise corrections (CP), without counterpoise corrections (noCP), as well as their average (AVG). The last row contains data for the M06-L density functional in the aTZ basis set for comparison to the B97M-V results.

kcal/mol	BF	CP RMSD	noCP RMSD	AVG RMSD	CP MSE	noCP MSE	AVG MSE
DZ	321	0.75	1.91	0.67	0.64	-1.45	-0.41
TZ	724	0.40	0.75	0.34	0.30	-0.54	-0.12
aDZ	536	0.44	0.55	0.31	0.34	-0.35	-0.01
aTZ	1127	0.33	0.23	0.26	0.24	0.04	0.14
pc1	321	0.53	1.81	0.95	0.15	-1.46	-0.66
pc2	724	0.36	0.27	0.25	0.27	-0.05	0.11
apc1	536	0.55	2.15	0.95	0.43	-1.68	-0.62
apc2	1127	0.34	0.40	0.25	0.25	-0.18	0.04
SVP	321	0.53	2.05	0.89	0.44	-1.56	-0.56
SVPD	474	0.34	1.57	0.70	0.26	-1.21	-0.48
TZVP	655	0.37	0.41	0.29	0.24	-0.21	0.01
TZVPD	808	0.35	0.25	0.28	0.28	0.07	0.17
LP	939	0.38	0.35	0.29	0.28	-0.09	0.09
aQZ	2026	0.34	0.27	0.30	0.25	0.15	0.20
QZVPD	1566	0.34	0.31	0.32	0.26	0.20	0.23
aTZ*	1127	1.08	0.43	0.73	0.96	0.30	0.63

as the CP and noCP RMSDs for the aTZ basis set differ by no more than 0.02 kcal/mol. While the noCP aTZ RMSD is 0.19 kcal/mol, the lowest possible RMSD is achieved in the TZVPD basis set without counterpoise corrections (0.18 kcal/mol). According to the S66 data, 2 basis sets that are substantially smaller than aTZ can be employed without counterpoise corrections to match the quality of the noCP aTZ result: pc2 and TZVPD. In addition, it appears that a variety of even smaller basis sets can be employed with counterpoise corrections: pc2, apc2, SVPD, and TZVPD. **Based on the results from the A24, S22, and S66 datasets, the def2-SVPD basis set (to be used with counterpoise corrections) and the def2-TZVPD basis set (to be used without counterpoise corrections) can be recommended as alternatives to the non-counterpoise-corrected aug-cc-pVTZ basis set for non-covalent interactions. Furthermore, for systems where the use of diffuse functions may lead to issues with linear dependence, the pc-2 basis set is recommended for use without counterpoise corrections.**

4.2 Grids

Different density functionals converge to their "infinite grid" limit at different rates. To ensure that B97M-V does not converge too slowly, it was mentioned in Section 2.5 that the billions of fits were filtered such that the least-squares fit energies generated in the (99,590)/SG-1 and (250,590)/SG-1 grids differed by a maximum of 0.01 kcal/mol. The effectiveness of this decision is tested by analyzing the grid sensitivity of B97M-V relative to other density functionals on the methane dimer PEC from NBC10-2, calculated in the aTZ basis set. The results are shown in Figure 6, with the associated maximum absolute deviations (with respect to the (250,590) grid) in cal/mol in Table 19. For the VV10 NLC functional, the SG-1 grid is used and not varied.

The B97M-V PEC looks nearly acceptable in the SG-1 grid, and is fully converged in

Table 18: RMSDs and MSEs in kcal/mol for the S66 dataset computed in 15 basis sets. The abbreviations are explained in Section 4.1. The second column contains the number of basis functions (BF) for the largest interaction in S66: the pentane dimer. The interactions were computed with the (75,302)/SG-0 grid with counterpoise corrections (CP), without counterpoise corrections (noCP), as well as their average (AVG). The last row contains data for the M06-L density functional in the aTZ basis set for comparison to the B97M-V results.

kcal/mol	BF	CP RMSD	noCP RMSD	AVG RMSD	CP MSE	noCP MSE	AVG MSE
DZ	260	0.67	1.69	0.66	0.52	-1.39	-0.43
TZ	636	0.32	0.73	0.31	0.21	-0.60	-0.19
aDZ	446	0.28	0.54	0.28	0.19	-0.43	-0.12
aTZ	1012	0.21	0.19	0.17	0.13	-0.04	0.05
pc1	260	0.37	1.34	0.66	0.10	-1.21	-0.56
pc2	636	0.22	0.21	0.15	0.15	-0.13	0.01
apc1	446	0.35	1.58	0.69	0.28	-1.35	-0.54
apc2	1012	0.21	0.32	0.19	0.13	-0.20	-0.03
SVP	260	0.49	1.75	0.78	0.36	-1.46	-0.55
SVPD	392	0.21	1.21	0.55	0.14	-1.10	-0.48
TZVP	454	0.24	0.39	0.22	0.13	-0.28	-0.08
TZVPD	586	0.22	0.18	0.18	0.16	-0.02	0.07
LP	822	0.24	0.25	0.18	0.15	-0.14	0.00
aQZ	1904	0.22	0.18	0.19	0.14	0.05	0.09
QZVPD	1422	0.22	0.20	0.21	0.14	0.10	0.12
aTZ*	1012	0.81	0.36	0.55	0.74	0.17	0.46

the (75,302) grid. The same can be said for all of the density functionals, except M06-L, M06, and M11. The density functional with the smallest MAX in the SG-1 grid (11.36 cal/mol) is ωB97X-V, while B97M-V and the non-empirical PBE density functional have maximum absolute deviations of approximately 27 cal/mol. For comparison, the least grid-sensitive Minnesota density functional (M06-2X) has a MAX of around 45 cal/mol in the SG-1 grid, with M11, M06-L, and M06 having deviations between 146 and 190 cal/mol. In the (75,302) grid, the MAX for most of the density functionals drops below 10 cal/mol. The outliers include M06-L, M06, and M11, and this result is repeated in the (99,590) grid. In fact, the M06 potential energy curve computed with the finest grid does not exhibit a proper well shape, indicating that it is not at its "infinite grid" limit even with the (250,590) grid. Furthermore, the strange behavior that was seen for M11-L with the benzene-argon dimer is much more pronounced in the case of the methane dimer, and it is clear that the feature cannot be eliminated by using a finer grid.

B97M-V is the only semi-empirical meta-GGA density functional out of those considered that is as grid-insensitive as its GGA counterparts. In fact, in the (75,302) grid, its MAX (4.57 cal/mol) is considerably smaller than that of 3 of the tested GGA density functionals: B97-D (10.79 cal/mol), B97-D2 (6.77 cal/mol), and ωB97X-D (6.81 cal/mol). Furthermore, out of the 8 meta-GGA density functionals considered, B97M-V is the least grid-sensitive density functional (even when compared to the non-empirical TPSS density functional).

Based on the data from Figure 6 and Table 19, it appears as if the (75,302)/SG-1 grid can be recommended for B97M-V. However, the methane dimer test only covers a very small fraction of the types of interactions that B97M-V can be applied to. In order to be absolutely certain of this recommendation, all of the data points in the training, primary test, and secondary test sets (with the exception of the absolute atomic energies and the rare-gas dimer PECs) were computed with the following grids:

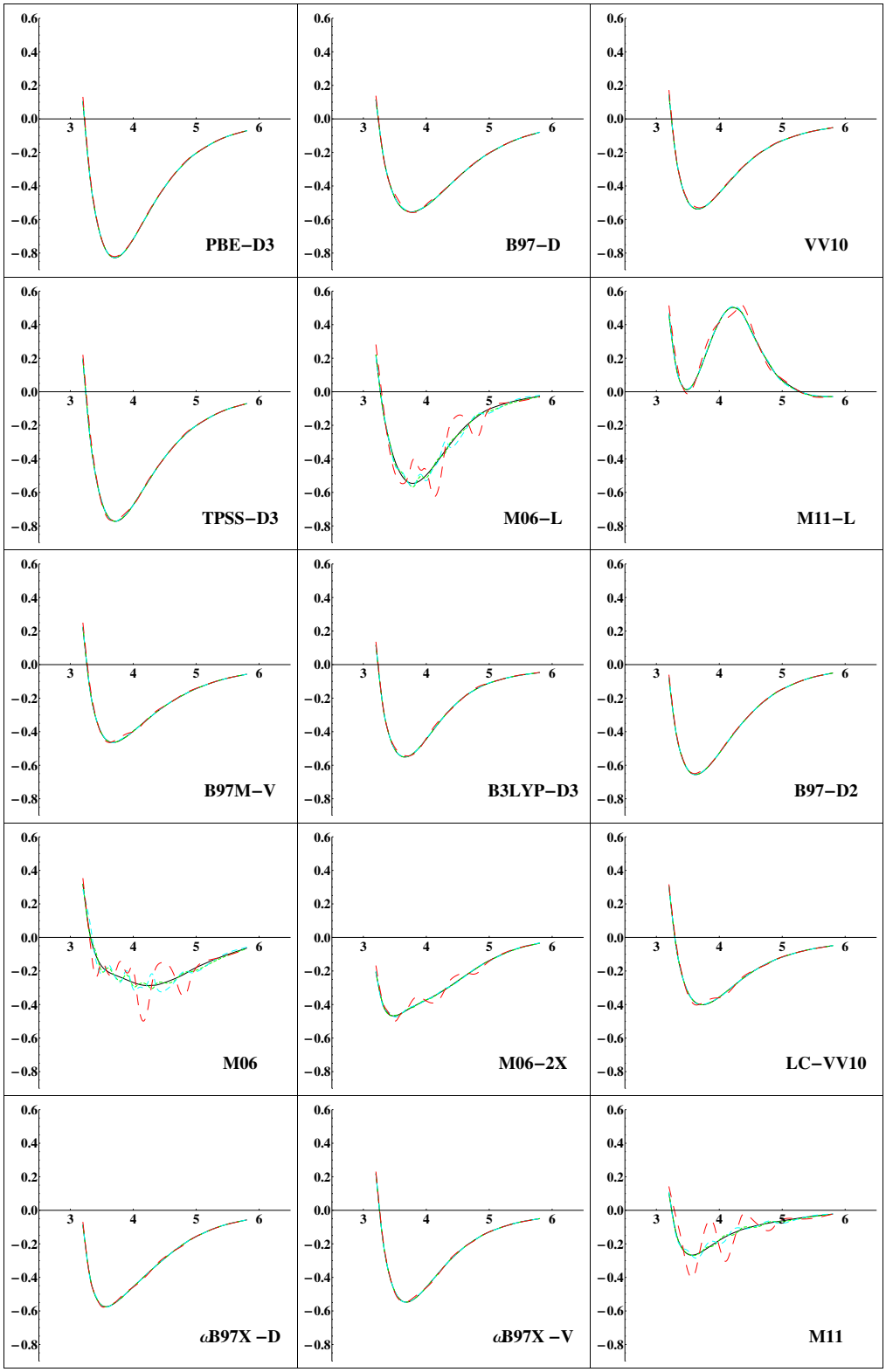

Figure 6: Methane dimer potential energy curves for 15 density functionals with 4 different local exchange-correlation grids (SG-1, (75,302), (99,590), and (250,590)), calculated in the aug-cc-pVTZ basis set without counterpoise corrections. The x-axis shows bond length in Å and the y-axis shows binding energy in kcal/mol. The color scheme is as follows: SG-1 (Red with Large Dashes), (75,302) (Cyan; Medium Dashes), (99,590) (Green; Small Dashes), (250,590) (Black; No Dashes). For the VV10 NLC functional, the SG-1 grid is used and not varied.

Table 19: Maximum absolute deviations in cal/mol for the 18 points on the methane dimer potential energy curve from NBC10-2. The deviations are taken with respect to the (250,590) grid results. For the VV10 NLC functional, the SG-1 grid is used and not varied.

cal/mol	SG-1	(75,302)	(99,590)
PBE-D3	27.06	4.39	0.34
B97-D	22.62	10.79	1.97
VV10	27.94	4.44	0.68
TPSS-D3	34.77	7.91	2.12
M06-L	165.54	56.24	23.32
M11-L	54.86	8.82	5.66
B97M-V	27.79	4.57	1.52
B3LYP-D3	19.61	3.75	0.40
B97-D2	18.90	6.77	1.10
M06	189.29	68.93	29.78
M06-2X	44.84	11.49	4.87
LC-VV10	20.17	3.25	1.01
ωB97X-D	18.89	6.81	2.11
ωB97X-V	11.36	1.91	0.57
M11	146.59	24.55	10.61

SG-1/SG-1, (75,302)/SG-1, (99,590)/SG-1, and (250,590)/SG-1.

Table 20 summarizes the results of this comprehensive test, which are categorized with respect to 3 metrics: absolute percent error (APE), absolute error (AE), as well as their product (APE·AE). With the assumption that the (250,590)/SG-1 results are fully converged with respect to the grid, Table 20 was populated with data from the aforementioned 2329 data points from the training, primary test, and secondary test sets. Starting with the (99,590)/SG-1 grid, it is clear that the filtering applied during the training stage has completely transferred to the final functional form, since all 2329 data points have absolute errors less than 0.01 kcal/mol. The SG-1/SG-1 results are clearly unacceptable, with 9 data points having APEs larger than 100% and 507 data points having an AE of more than 0.1 kcal/mol. The (75,302)/SG-1 grid strikes a reasonable balance between the SG-1/SG-1 and (99,590)/SG-1 grids, and the largest absolute errors are no greater than 0.1 kcal/mol. However, an outlier appears that has an APE of more than 50%. This specific data point is in the S22x5 dataset and corresponds to the parallel-displaced benzene dimer at a separation of 2.0·R_e. This data point was investigated further in order to identify grids that can reduce this outlying APE.

Table 21 contains the APEs for this investigation in a variety of radial (columns) and angular (rows) grids. The APEs are calculated with respect to the (500,974)/SG-1 grid and it is clear that the accuracy for this specific data point relies entirely on the number of angular grid points. Accordingly, the coarsest grid that can substantially reduce the 55.6% error of the (75,302)/SG-1 grid is the (75,590)/SG-1 grid, which reduces the APE to less than 3%. As a consequence of this test, the (75,590)/SG-1 grid was added to Table 20 in order to assess its performance for the remaining 2328 data points. As predicted, the (75,590)/SG-1 grid substantially improves upon the coarser (75,302)/SG-1 grid, with a maximum APE of only 5.5% for all 2329 data points.

Finally, in order to test the sensitivity of the VV10 NLC functional to the integration grid, the SG-0 grid was used for the nonlocal integration, along with the (75,302) grid for the integration of the local component of B97M-V. A comparison of the (75,302)/SG-0 and (75,302)/SG-1 grids in Table 20 indicates that the integration of the VV10 NLC functional is not very sensitive to the grid, and the SG-0 grid can be applied if necessary. **Based on these results, the (75,302)/SG-0 and (75,302)/SG-1 grids are recommended as the bare minimum for use with B97M-V (particularly for quick calculations), while the (99,590)/SG-1 grid is recommended if results near the "infinite grid" limit are required. Finally, the (75,590)/SG-1 grid can serve as a compromise between these 2 limits.**

4.3 Timings

Since B97M-V does not contain any exact exchange, it has the potential of being much faster than its hybrid counterparts. However,

Table 20: Error ranges for 2329 data points from the training, primary test, and secondary tests sets. From the original 2460 data points, the 8 data points from AE8 as well as the 123 data points corresponding to the rare-gas dimer PECs were dropped. The errors are taken with respect to the (250,590)/SG-1 grid. The grids are assessed with respect to 3 metrics: absolute percent error (APE), absolute error (AE), as well as their product (APE·AE).

APE (%)	[0,1)	[1,2)	[2,5)	[5,10)	[10,50)	[50,100)	[100,∞)
SG-1/SG-1	1699	233	213	67	82	26	9
(75,302)/SG-0	2184	87	40	9	8	1	0
(75,302)/SG-1	2213	72	25	12	6	1	0
(75,590)/SG-1	2298	22	7	2	0	0	0
(99,590)/SG-1	2328	1	0	0	0	0	0
AE (kcal/mol)	[0,0.01)	[0.01,0.02)	[0.02,0.05)	[0.05,0.10)	[0.1,0.5)	[0.5,1)	[1,∞)
SG-1/SG-1	623	320	517	362	441	52	14
(75,302)/SG-0	1950	246	119	14	0	0	0
(75,302)/SG-1	1996	238	87	8	0	0	0
(75,590)/SG-1	2270	47	12	0	0	0	0
(99,590)/SG-1	2329	0	0	0	0	0	0
APE·AE (%·kcal/mol)	[0,0.1)	[0.1,0.2)	[0.2,0.5)	[0.5,1)	[1,5)	[5,10)	[10,∞)
SG-1/SG-1	1900	98	109	66	96	16	44
(75,302)/SG-0	2303	13	7	4	2	0	0
(75,302)/SG-1	2309	9	7	3	1	0	0
(75,590)/SG-1	2327	2	0	0	0	0	0
(99,590)/SG-1	2329	0	0	0	0	0	0

Table 21: Absolute percent errors (APE) for the S22x5 parallel-displaced benzene dimer at a separation of 2.0·R_e for a variety of radial (columns) and angular (rows) grids. The APE is calculated with respect to the binding energy in the (500,974) grid. The SG-1 grid is used throughout for integrating the VV10 NLC functional. For reference, the APE for the SG-1/SG-1 grid is 243.9%.

APE (%)	75	87	99	150	250	500
302	55.6	56.2	52.7	53.9	54.0	54.0
350	19.7	19.8	20.3	19.3	19.3	19.3
434	20.1	20.6	16.9	20.0	19.9	19.9
590	2.9	3.3	3.4	3.2	3.2	3.2
770	1.0	0.4	1.0	1.1	1.0	1.0
974	0.2	0.2	0.1	0.0	0.0	0.0

the VV10 NLC functional requires additional grid point evaluations and as a result, B97M-V will be slightly slower than a local meta-GGA density functional like M06-L (for a single Fock build). In order to quantify the additional time required to evaluate the VV10 NLC functional, as a well as to compare the effect of using different grids, timings for a single Fock build were carried out with B97-D, B97M-V, M06-L, and M06-2X. For B97M-V, 3 different grids were used ((75,302)/SG-0, (75,302)/SG-1, and (99,590)/SG-1), while the rest of the density functionals employed the (75,302) grid. The resulting timings, shown in Figure 7, are taken as a ratio to the B97-D result, which is the cheapest density functional of the 4 tested. The molecules considered were $(H_2O)_n$ for $n = 2, 4, 8, 16$ in 2 basis sets: LP and aTZ. The results indicate that the additional cost of evaluating the VV10 NLC functional is negligible, when either the SG-0 or SG-1 grids are used in conjunction with the (75,302) grid for the local component. Using the (99,590) grid for the local component of B97M-V is very

costly and mostly unnecessary according to the results from the previous section.

As a reference value for those interested in implementing this new density functional, the absolute energy (in hartrees) of hydrogen fluoride (HF) with a bond length of 0.9158 Å in the aug-cc-pVTZ basis set with the (75,302)/SG-1 grid is -100.4472797104.

5 Conclusions

The primary goal of the development of the B97M-V density functional was to create a minimally-parameterized and highly-transferable local meta-GGA density functional that could predict accurate energetics for both bonded and non-bonded interactions. The most important aspects of the development process, and the resulting density functional, may be summarized as follows:

Table 22: Density functionals ranked based on their overall unweighted RMSDs in kcal/mol for all thermochemistry (Columns 1-2) and non-covalent interactions (Columns 3-4) data points from the training, primary test, and secondary test sets.

Functional	TC RMSD	Functional	NC RMSD
M06-2X	3.21	B97M-V	0.22
ωB97X-V	3.60	ωB97X-V	0.32
ωB97X-D	3.61	M06-L	0.42
B97M-V	3.93	B97-D2	0.48
B97-D2	3.97	ωB97X-D	0.54
M11	3.97	M11	0.55
M06	4.18	M06	0.57
B3LYP-D3	4.66	LC-VV10	0.72
B97-D	5.56	M06-2X	0.77
M06-L	5.63	B3LYP-D3	0.77
TPSS-D3	6.45	B97-D	0.82
M11-L	6.68	TPSS-D3	0.85
LC-VV10	6.79	M11-L	1.08
VV10	9.81	PBE-D3	1.23
PBE-D3	10.10	VV10	1.36

1. Unlike the development of most meta-GGA density functionals, where only one or a small number of functional forms are considered, a combinatorial screening approach was applied to the density functional design problem. Out of a space

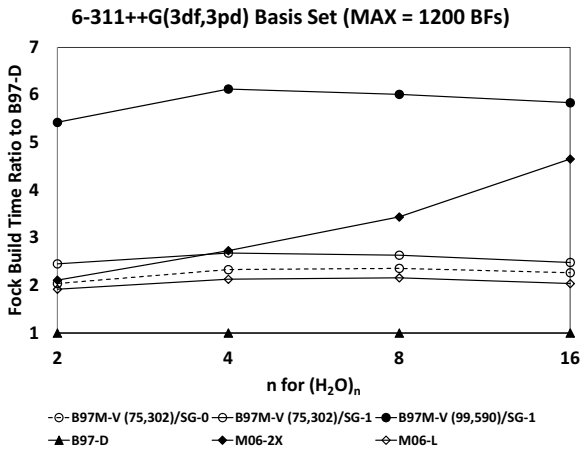

(a)

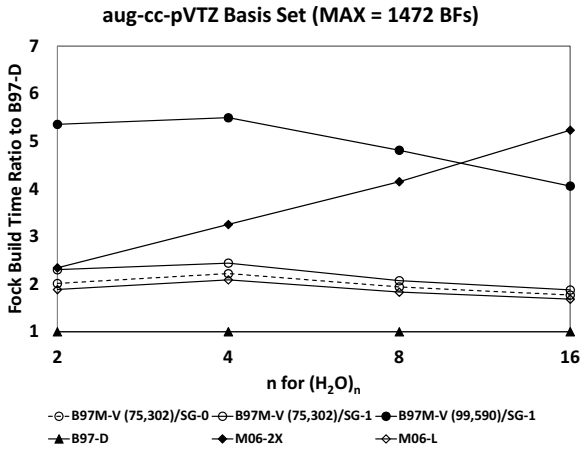

(b)

Figure 7: Single Fock build timings for B97-D, B97M-V, M06-L, and M06-2X for water clusters of varying size in 2 different basis sets: 6-311++G(3df,3pd) and aug-cc-pVTZ. The timings are displayed as a ratio to the B97-D value. For B97-D, M06-2X, and M06-L, the (75,302) grid was used, while for B97M-V, timings for 3 different grid combinations are shown. The number of basis functions (BF) for the largest water cluster within each basis set is shown in the title of the associated plot.

of almost 10^{40} possible functional forms, over 10 billion were screened for optimal accuracy, transferability, numerical stability, and desired physical properties. The results are necessarily sensitive to the data used for training and testing (as well as the associated weights), which includes a wide range of main group thermochemistry and non-covalent interactions, but no transition metal systems or strong correlation cases.

2. From the partial search of the space of possible meta-GGA density functionals, many strong candidates emerged, and the best one (as measured by the defined criteria) has been self-consistently optimized. The resulting semi-empirical density functional, B97M-V, is a 12-parameter local meta-GGA density functional based on the B97 GGA and B00 meta-GGA models for local exchange and correlation, augmented with nonlocal correlation using the VV10 nonlocal correlation functional. Since it does not contain exact exchange, B97M-V complements the range-separated hybrid GGA ωB97X-V density functional that was recently developed from a complete search of a much smaller GGA functional space.

3. Detailed assessment against 14 existing density functionals on main group thermochemistry and non-covalent interactions suggests that B97M-V is the best density functional tested for non-bonded interactions by a very significant margin, even outperforming ωB97X-V. The RMSD of B97M-V for non-covalent interactions is almost 2 times smaller than that of the next best local density functional. Its performance for thermochemistry is also very good, 30% better than the next best local density functional tested. Table 22 ranks the 15 benchmarked density functionals with respect to their overall RMSDs for all of the bonded and non-bonded interactions in the training, primary test, and secondary test sets. These results suggest that B97M-V should be a useful improvement over existing local meta-GGA density functionals for a wide range of chemical applications, a conclusion which is supported by a large variety of additional tests conducted in this work.

4. As a semi-empirical density functional developed using a computationally efficient but physically inexact form, B97M-V also necessarily has significant weaknesses in some applications, despite the successes discussed above. The main weakness arises in predicting reaction barrier heights, where due to the lack of exact exchange, the RMSDs of B97M-V are 3 to 4 times larger than the best hybrid density functionals (though comparable to those of existing local meta-GGAs). It is also likely that B97M-V will perform poorly for relative energies that are sensitive to self-interaction (delocalization) error or for systems that exhibit strong correlations.

5. B97M-V was trained in the aug-cc-pVQZ basis set for thermochemistry and the aug-cc-pVTZ basis set (without counterpoise corrections) for non-covalent interactions. Its basis set dependence has been thoroughly tested in order to identify smaller basis sets that can provide results similar in quality to those acquired with the basis sets used for training the parameters. For thermochemistry, the cc-pVQZ, 6-311++G(3df,3pd), pc-2, pc-3, and def2-QZVP basis sets can be recommended as smaller alternatives to the aug-cc-pVQZ basis set. For non-covalent interactions, the def2-SVPD basis set used with counterpoise corrections and the def2-TZVPD basis set used without counterpoise corrections can be recommended as smaller alternatives to the non-counterpoise-corrected aug-cc-pVTZ basis set. Furthermore, for systems where the use of diffuse functions may lead to issues with linear dependence, the pc-2 basis set is recommended for use without counterpoise corrections. It is important to note that while B97M-V was

trained very close to the basis set limit for thermochemistry, it was not necessarily trained at the basis set limit for noncovalent interactions.

6. Since existing semi-empirical meta-GGA density functionals are very sensitive to the integration grid, B97M-V was trained with the goal of making the (99,590)/SG-1 grid the "infinite grid" limit. The (75,302)/SG-0 and (75,302)/SG-1 grids are recommended as the bare minimum for use with B97M-V (particularly for quick calculations), while the (99,590)/SG-1 grid is recommended if results near the "infinite grid" limit are required. Finally, the (75,590)/SG-1 grid can serve as a compromise between these 2 limits.

7. It is desirable to apply the same training approach used here to develop other semi-empirical density functionals with improved physical content, so that the resulting density functionals are likewise minimally parameterized and optimally transferable. Perhaps the most obvious candidate is a meta-GGA that includes nonlocal exchange through range-separation. We hope to report such a development in due course.

6 Acknowledgements

NM would like to thank Jonathan Thirman for help with the parallel implementation of the least-squares fitting code and Jonathon Witte for providing a useful script for analyzing geometries. This work was supported by the Director, Office of Energy Research, Office of Basic Energy Sciences, Chemical Sciences Division of the U.S. Department of Energy under Contract DE-AC0376SF00098, with additional support under Award No. DE-FG02-12ER16362.

References

(1) Kohn, W.; Sham, L. J. Self-Consistent Equations Including Exchange and Correlation Effects. *Phys. Rev.* **1965**, *140*, A1133–A1138.

(2) Kohn, W.; Becke, A. D.; Parr, R. G. Density Functional Theory of Electronic Structure. *The Journal of Physical Chemistry* **1996**, *100*, 12974–12980.

(3) Perdew, J. P.; Ruzsinszky, A.; Tao, J.; Staroverov, V. N.; Scuseria, G. E.; Csonka, G. I. Prescription for the design and selection of density functional approximations: More constraint satisfaction with fewer fits. *The Journal of Chemical Physics* **2005**, *123*, 062201.

(4) Gill, P. M. W.; Loos, P.-F. Uniform electron gases. *Theoretical Chemistry Accounts* **2011**, *131*.

(5) Perdew, J. P.; Burke, K.; Ernzerhof, M. Generalized Gradient Approximation Made Simple. *Phys. Rev. Lett.* **1996**, *77*, 3865–3868.

(6) Grimme, S. Semiempirical GGA-type density functional constructed with a long-range dispersion correction. *Journal of Computational Chemistry* **2006**, *27*, 1787–1799.

(7) Negele, J. W.; Vautherin, D. Density-Matrix Expansion for an Effective Nuclear Hamiltonian. *Phys. Rev. C* **1972**, *5*, 1472–1493.

(8) Perdew, J. P.; Kurth, S.; Zupan, A.; Blaha, P. Accurate Density Functional with Correct Formal Properties: A Step Beyond the Generalized Gradient Approximation. *Phys. Rev. Lett.* **1999**, *82*, 2544–2547.

(9) Becke, A. D. Density-functional thermochemistry. III. The role of exact exchange. *The Journal of Chemical Physics* **1993**, *98*, 5648–5652.

(10) Becke, A. D. A new mixing of Hartree–Fock and local density-functional theories. *The Journal of Chemical Physics* **1993**, *98*, 1372–1377.

(11) Becke, A. D. Density-functional exchange-energy approximation with correct asymptotic behavior. *Phys. Rev. A* **1988**, *38*, 3098–3100.

(12) Perdew, J. P.; Chevary, J. A.; Vosko, S. H.; Jackson, K. A.; Pederson, M. R.; Singh, D. J.; Fiolhais, C. Atoms, molecules, solids, and surfaces: Applications of the generalized gradient approximation for exchange and correlation. *Phys. Rev. B* **1992**, *46*, 6671–6687.

(13) Mardirossian, N.; Head-Gordon, M. Exploring the limit of accuracy for density functionals based on the generalized gradient approximation: Local, global hybrid, and range-separated hybrid functionals with and without dispersion corrections. *The Journal of Chemical Physics* **2014**, *140*, 18A527.

(14) Wellendorff, J.; Lundgaard, K. T.; Jacobsen, K. W.; Bligaard, T. mBEEF: An accurate semi-local Bayesian error estimation density functional. *The Journal of Chemical Physics* **2014**, *140*, 144107.

(15) Becke, A. D. Local exchange-correlation approximations and first-row molecular dissociation energies. *International Journal of Quantum Chemistry* **1985**, *27*, 585–594.

(16) Becke, A. D. Correlation energy of an inhomogeneous electron gas: A coordinate-space model. *The Journal of Chemical Physics* **1988**, *88*, 1053–1062.

(17) Becke, A. D.; Roussel, M. R. Exchange holes in inhomogeneous systems: A coordinate-space model. *Phys. Rev. A* **1989**, *39*, 3761–3767.

(18) Becke, A. D. Density-functional thermochemistry. IV. A new dynamical correlation functional and implications for exact-exchange mixing. *The Journal of Chemical Physics* **1996**, *104*, 1040–1046.

(19) Becke, A. D. Density-functional thermochemistry. V. Systematic optimization of exchange-correlation functionals. *The Journal of Chemical Physics* **1997**, *107*, 8554–8560.

(20) Becke, A. D. A new inhomogeneity parameter in density-functional theory. *The Journal of Chemical Physics* **1998**, *109*, 2092–2098.

(21) Schmider, H. L.; Becke, A. D. Density functionals from the extended G2 test set: Second-order gradient corrections. *The Journal of Chemical Physics* **1998**, *109*, 8188–8199.

(22) Becke, A. D. Exploring the limits of gradient corrections in density functional theory. *J. Comput. Chem.* **1999**, *20*, 63–69.

(23) Becke, A. D. Simulation of delocalized exchange by local density functionals. *The Journal of Chemical Physics* **2000**, *112*, 4020–4026.

(24) Proynov, E.; Vela, A.; Salahub, D. Nonlocal correlation functional involving the Laplacian of the density. *Chemical Physics Letters* **1994**, *230*, 419 – 428.

(25) Colle, R.; Salvetti, O. Approximate calculation of the correlation energy for the closed shells. *Theoretical Chemistry Accounts: Theory, Computation, and Modeling (Theoretica Chimica Acta)* **1975**, *37*, 329–334.

(26) Proynov, E. I.; Sirois, S.; Salahub, D. R. Extension of the LAP functional to include parallel spin correlation. *Int. J. Quantum Chem.* **1997**, *64*, 427–446.

(27) Proynov, E.; Chermette, H.; Salahub, D. R. New tau-dependent correlation functional combined with a modified Becke exchange. *The Journal of Chemical Physics* **2000**, *113*, 10013–10027.

(28) Handy, N. C.; Cohen, A. J. Left-right correlation energy. *Molecular Physics* **2001**, *99*, 403–412.

(29) Proynov, E. I.; Thakkar, A. J. Is combining meta-GGA correlation functionals with the OPTX exchange functional useful? *Int. J. Quantum Chem.* **2006**, *106*, 436–446.

(30) Zhang, Y.; Salahub, D. R. A reparametrization of a meta-GGA exchange-correlation functional with improved descriptions of van der Waals interactions. *Chemical Physics Letters* **2007**, *436*, 394 – 399.

(31) Zhang, Y.; Vela, A.; Salahub, D. Reparameterization of a meta-generalized gradient approximation functional by combining TPSS exchange with 1 correlation. *Theoretical Chemistry Accounts* **2007**, *118*, 693–707.

(32) Koehl, R. M.; Odom, G. K.; Scuseria, G. E. The use of density matrix expansions for calculating molecular exchange energies. *Molecular Physics* **1996**, *87*, 835–843.

(33) Voorhis, T. V.; Scuseria, G. E. Exchange energy functionals based on the density matrix expansion of the Hartree-Fock exchange term. *Molecular Physics* **1997**, *92*, 601–608.

(34) Voorhis, T. V.; Scuseria, G. E. A novel form for the exchange-correlation energy functional. *The Journal of Chemical Physics* **1998**, *109*, 400–410.

(35) Kurth, S.; Perdew, J. P.; Blaha, P. Molecular and solid-state tests of density functional approximations: LSD, GGAs, and meta-GGAs. *Int. J. Quantum Chem.* **1999**, *75*, 889–909.

(36) Tao, J.; Perdew, J. P.; Staroverov, V. N.; Scuseria, G. E. Climbing the Density Functional Ladder: Nonempirical Meta˘Generalized Gradient Approximation Designed for Molecules and Solids. *Phys. Rev. Lett.* **2003**, *91*, 146401.

(37) Staroverov, V. N.; Scuseria, G. E.; Tao, J.; Perdew, J. P. Comparative assessment of a new nonempirical density functional: Molecules and hydrogen-bonded complexes. *The Journal of Chemical Physics* **2003**, *119*, 12129–12137.

(38) Perdew, J. P.; Ruzsinszky, A.; Tao, J.; Csonka, G. I.; Scuseria, G. E. One-parameter optimization of a nonempirical meta-generalized-gradient-approximation for the exchange-correlation energy. *Phys. Rev. A* **2007**, *76*, 042506.

(39) Perdew, J. P.; Ruzsinszky, A.; Csonka, G. I.; Constantin, L. A.; Sun, J. Workhorse Semilocal Density Functional for Condensed Matter Physics and Quantum Chemistry. *Phys. Rev. Lett.* **2009**, *103*, 026403.

(40) Ruzsinszky, A.; Sun, J.; Xiao, B.; Csonka, G. I. A meta-GGA Made Free of the Order of Limits Anomaly. *Journal of Chemical Theory and Computation* **2012**, *8*, 2078–2087.

(41) Sun, J.; Xiao, B.; Ruzsinszky, A. Communication: Effect of the orbital-overlap dependence in the meta generalized gradient approximation. *The Journal of Chemical Physics* **2012**, *137*, 051101.

(42) Hao, P.; Sun, J.; Xiao, B.; Ruzsinszky, A.; Csonka, G. I.; Tao, J.; Glindmeyer, S.; Perdew, J. P. Performance of meta-GGA Functionals on General Main Group Thermochemistry, Kinetics, and Noncovalent Interactions. *Journal of Chemical Theory and Computation* **2013**, *9*, 355–363.

(43) Sun, J.; Haunschild, R.; Xiao, B.; Bulik, I. W.; Scuseria, G. E.; Perdew, J. P. Semilocal and hybrid meta-generalized

gradient approximations based on the understanding of the kinetic-energy-density dependence. *The Journal of Chemical Physics* **2013**, *138*, 044113.

(44) Sun, J.; Xiao, B.; Fang, Y.; Haunschild, R.; Hao, P.; Ruzsinszky, A.; Csonka, G. I.; Scuseria, G. E.; Perdew, J. P. Density Functionals that Recognize Covalent, Metallic, and Weak Bonds. *Phys. Rev. Lett.* **2013**, *111*, 106401.

(45) Sun, J.; Perdew, J. P.; Ruzsinszky, A. Semilocal density functional obeying a strongly tightened bound for exchange. *Proceedings of the National Academy of Sciences* **2015**,

(46) Tao, J. Exchange energy density of an atom as a functional of the electron density. *The Journal of Chemical Physics* **2001**, *115*, 3519–3530.

(47) Tao, J. An accurate MGGA-based hybrid exchange-correlation functional. *The Journal of Chemical Physics* **2002**, *116*, 2335–2337.

(48) Lee, C.; Yang, W.; Parr, R. G. Development of the Colle-Salvetti correlation-energy formula into a functional of the electron density. *Phys. Rev. B* **1988**, *37*, 785–789.

(49) Toulouse, J.; Savin, A.; Adamo, C. Validation and assessment of an accurate approach to the correlation problem in density functional theory: The KrigerChenIafrateSavin model. *The Journal of Chemical Physics* **2002**, *117*, 10465–10473.

(50) Boese, A. D.; Handy, N. C. New exchange-correlation density functionals: The role of the kinetic-energy density. *The Journal of Chemical Physics* **2002**, *116*, 9559–9569.

(51) Boese, A. D.; Martin, J. M. L. Development of density functionals for thermochemical kinetics. *The Journal of Chemical Physics* **2004**, *121*, 3405–3416.

(52) Zhao, Y.; Truhlar, D. G. A new local density functional for main-group thermochemistry, transition metal bonding, thermochemical kinetics, and noncovalent interactions. *The Journal of Chemical Physics* **2006**, *125*, 194101.

(53) Peverati, R.; Truhlar, D. G. M11-L: A Local Density Functional That Provides Improved Accuracy for Electronic Structure Calculations in Chemistry and Physics. *The Journal of Physical Chemistry Letters* **2012**, *3*, 117–124.

(54) Zhao, Y.; Schultz, N. E.; Truhlar, D. G. Exchange-correlation functional with broad accuracy for metallic and nonmetallic compounds, kinetics, and noncovalent interactions. *The Journal of Chemical Physics* **2005**, *123*, 161103.

(55) Zhao, Y.; Schultz, N. E.; Truhlar, D. G. Design of Density Functionals by Combining the Method of Constraint Satisfaction with Parametrization for Thermochemistry, Thermochemical Kinetics, and Noncovalent Interactions. *Journal of Chemical Theory and Computation* **2006**, *2*, 364–382.

(56) Zhao, Y.; Truhlar, D. The M06 suite of density functionals for main group thermochemistry, thermochemical kinetics, noncovalent interactions, excited states, and transition elements: two new functionals and systematic testing of four M06-class functionals and 12 other functionals. *Theoretical Chemistry Accounts: Theory, Computation, and Modeling (Theoretica Chimica Acta)* **2008**, *120*, 215–241.

(57) Zhao, Y.; Truhlar, D. G. Density Functional for Spectroscopy: No Long-Range Self-Interaction Error, Good Performance for Rydberg and Charge-Transfer

States, and Better Performance on Average than B3LYP for Ground States. *The Journal of Physical Chemistry A* **2006**, *110*, 13126–13130.

(58) Zhao, Y.; Truhlar, D. G. Exploring the Limit of Accuracy of the Global Hybrid Meta Density Functional for Main-Group Thermochemistry, Kinetics, and Noncovalent Interactions. *Journal of Chemical Theory and Computation* **2008**, *4*, 1849–1868.

(59) Peverati, R.; Truhlar, D. G. Improving the Accuracy of Hybrid Meta-GGA Density Functionals by Range Separation. *The Journal of Physical Chemistry Letters* **2011**, *2*, 2810–2817.

(60) Hammer, B.; Hansen, L. B.; Nørskov, J. K. Improved adsorption energetics within density-functional theory using revised Perdew-Burke-Ernzerhof functionals. *Phys. Rev. B* **1999**, *59*, 7413–7421.

(61) del Campo, J. M.; Gázquez, J. L.; Trickey, S.; Vela, A. A new meta-GGA exchange functional based on an improved constraint-based {GGA}. *Chemical Physics Letters* **2012**, *543*, 179 – 183.

(62) Lin, Y.-S.; Tsai, C.-W.; Li, G.-D.; Chai, J.-D. Long-range corrected hybrid meta-generalized-gradient approximations with dispersion corrections. *The Journal of Chemical Physics* **2012**, *136*, 154109.

(63) Constantin, L. A.; Fabiano, E.; Della Sala, F. Meta-GGA Exchange-Correlation Functional with a Balanced Treatment of Nonlocality. *Journal of Chemical Theory and Computation* **2013**, *9*, 2256–2263.

(64) Constantin, L. A.; Fabiano, E.; Sala, F. D. Semilocal dynamical correlation with increased localization. *Phys. Rev. B* **2012**, *86*, 035130.

(65) Wellendorff, J.; Lundgaard, K. T.; Møgelhøj, A.; Petzold, V.; Landis, D. D.; Nørskov, J. K.; Bligaard, T.; Jacobsen, K. W. Density functionals for surface science: Exchange-correlation model development with Bayesian error estimation. *Phys. Rev. B* **2012**, *85*, 235149.

(66) Lee, K.; Murray, E. D.; Kong, L.; Lundqvist, B. I.; Langreth, D. C. Higher-accuracy van der Waals density functional. *Phys. Rev. B* **2010**, *82*, 081101.

(67) Perdew, J. P.; Ruzsinszky, A.; Csonka, G. I.; Vydrov, O. A.; Scuseria, G. E.; Constantin, L. A.; Zhou, X.; Burke, K. Restoring the Density-Gradient Expansion for Exchange in Solids and Surfaces. *Phys. Rev. Lett.* **2008**, *100*, 136406.

(68) Kristyan, S.; Pulay, P. Can (semi)local density functional theory account for the London dispersion forces? *Chemical Physics Letters* **1994**, *229*, 175 – 180.

(69) Hobza, P.; Šponer, J.; Reschel, T. Density functional theory and molecular clusters. *J. Comput. Chem.* **1995**, *16*, 1315–1325.

(70) Grimme, S. Accurate description of van der Waals complexes by density functional theory including empirical corrections. *J. Comput. Chem.* **2004**, *25*, 1463–1473.

(71) Grimme, S.; Antony, J.; Ehrlich, S.; Krieg, H. A consistent and accurate ab initio parametrization of density functional dispersion correction (DFT-D) for the 94 elements H-Pu. *The Journal of Chemical Physics* **2010**, *132*, 154104.

(72) Dion, M.; Rydberg, H.; Schröder, E.; Langreth, D. C.; Lundqvist, B. I. Van der Waals Density Functional for General Geometries. *Phys. Rev. Lett.* **2004**, *92*, 246401.

(73) Vydrov, O. A.; Wu, Q.; Voorhis, T. V. Self-consistent implementation of a nonlocal van der Waals density functional with a Gaussian basis set. *The Journal of Chemical Physics* **2008**, *129*, 014106.

(74) Vydrov, O. A.; Van Voorhis, T. Nonlocal van der Waals Density Functional Made Simple. *Phys. Rev. Lett.* **2009**, *103*, 063004.

(75) Vydrov, O. A.; Voorhis, T. V. Improving the accuracy of the nonlocal van der Waals density functional with minimal empiricism. *The Journal of Chemical Physics* **2009**, *130*, 104105.

(76) Vydrov, O. A.; Voorhis, T. V. Nonlocal van der Waals density functional: The simpler the better. *The Journal of Chemical Physics* **2010**, *133*, 244103.

(77) Vydrov, O. A.; Voorhis, T. V. Implementation and assessment of a simple nonlocal van der Waals density functional. *The Journal of Chemical Physics* **2010**, *132*, 164113.

(78) Vydrov, O. A.; Van Voorhis, T. Dispersion interactions from a local polarizability model. *Phys. Rev. A* **2010**, *81*, 062708.

(79) Klimeš, J.; Michaelides, A. Perspective: Advances and challenges in treating van der Waals dispersion forces in density functional theory. *The Journal of Chemical Physics* **2012**, *137*, 120901.

(80) Becke, A. D. Density functional calculations of molecular bond energies. *The Journal of Chemical Physics* **1986**, *84*, 4524–4529.

(81) Ceperley, D. M.; Alder, B. J. Ground State of the Electron Gas by a Stochastic Method. *Phys. Rev. Lett.* **1980**, *45*, 566–569.

(82) Perdew, J. P.; Wang, Y. Accurate and simple analytic representation of the electron-gas correlation energy. *Phys. Rev. B* **1992**, *45*, 13244–13249.

(83) Vosko, S. H.; Wilk, L.; Nusair, M. Accurate spin-dependent electron liquid correlation energies for local spin density calculations: a critical analysis. *Can. J. Phys.* **1980**, *58*, 1200–1211.

(84) Stoll, H.; Golka, E.; Preuß, H. Correlation energies in the spin-density functional formalism. *Theoretical Chemistry Accounts: Theory, Computation, and Modeling (Theoretica Chimica Acta)* **1980**, *55*, 29–41.

(85) Mardirossian, N.; Head-Gordon, M. ωB97X-V: A 10-parameter, range-separated hybrid, generalized gradient approximation density functional with nonlocal correlation, designed by a survival-of-the-fittest strategy. *Phys. Chem. Chem. Phys.* **2014**, *16*, 9904–9924.

(86) Lao, K. U.; Herbert, J. M. Accurate and Efficient Quantum Chemistry Calculations for Noncovalent Interactions in Many-Body Systems: The XSAPT Family of Methods. *The Journal of Physical Chemistry A* **2015**, *119*, 235–252.

(87) Karton, A.; Daon, S.; Martin, J. M. W4-11: A high-confidence benchmark dataset for computational thermochemistry derived from first-principles {W4} data. *Chemical Physics Letters* **2011**, *510*, 165 – 178.

(88) Zheng, J.; Zhao, Y.; Truhlar, D. G. Representative Benchmark Suites for Barrier Heights of Diverse Reaction Types and Assessment of Electronic Structure Methods for Thermochemical Kinetics. *Journal of Chemical Theory and Computation* **2007**, *3*, 569–582.

(89) Karton, A.; Tarnopolsky, A.; Lamère, J.-F.; Schatz, G. C.; Martin, J. M. L. Highly Accurate First-Principles Benchmark Data Sets for the Parametrization and Validation of Density Functional and Other Approximate Methods.

Derivation of a Robust, Generally Applicable, Double-Hybrid Functional for Thermochemistry and Thermochemical Kinetics. *The Journal of Physical Chemistry A* **2008**, *112*, 12868–12886.

(90) Lynch, B. J.; Zhao, Y.; Truhlar, D. G. Effectiveness of Diffuse Basis Functions for Calculating Relative Energies by Density Functional Theory. *The Journal of Physical Chemistry A* **2003**, *107*, 1384–1388.

(91) Chakravorty, S. J.; Gwaltney, S. R.; Davidson, E. R.; Parpia, F. A.; Fischer, C. F. Ground-state correlation energies for atomic ions with 3 to 18 electrons. *Phys. Rev. A* **1993**, *47*, 3649–3670.

(92) Mardirossian, N.; Lambrecht, D. S.; McCaslin, L.; Xantheas, S. S.; Head-Gordon, M. The Performance of Density Functionals for Sulfate-Water Clusters. *Journal of Chemical Theory and Computation* **2013**, *9*, 1368–1380.

(93) Sherrill, C. D.; Takatani, T.; Hohenstein, E. G. An Assessment of Theoretical Methods for Nonbonded Interactions: Comparison to Complete Basis Set Limit Coupled-Cluster Potential Energy Curves for the Benzene Dimer, the Methane Dimer, BenzeneMethane, and BenzeneH2S. *The Journal of Physical Chemistry A* **2009**, *113*, 10146–10159.

(94) Marshall, M. S.; Burns, L. A.; Sherrill, C. D. Basis set convergence of the coupled-cluster correction, delta[sub MP2][sup CCSD(T)]: Best practices for benchmarking non-covalent interactions and the attendant revision of the S22, NBC10, HBC6, and HSG databases. *The Journal of Chemical Physics* **2011**, *135*, 194102.

(95) Crittenden, D. L. A Systematic CCSD(T) Study of Long-Range and Noncovalent Interactions between Benzene and a Series of First- and Second-Row Hydrides and Rare Gas Atoms. *The Journal of Physical Chemistry A* **2009**, *113*, 1663–1669.

(96) Copeland, K. L.; Tschumper, G. S. Hydrocarbon/Water Interactions: Encouraging Energetics and Structures from DFT but Disconcerting Discrepancies for Hessian Indices. *Journal of Chemical Theory and Computation* **2012**, *8*, 1646–1656.

(97) Jurečka, P.; Šponer, J.; Černý, J.; Hobza, P. Benchmark database of accurate (MP2 and CCSD(T) complete basis set limit) interaction energies of small model complexes, DNA base pairs, and amino acid pairs. *Phys. Chem. Chem. Phys.* **2006**, *8*, 1985–1993.

(98) Karton, A.; Gruzman, D.; Martin, J. M. L. Benchmark Thermochemistry of the CnH2n+2 Alkane Isomers (n = 28) and Performance of DFT and Composite Ab Initio Methods for Dispersion-Driven Isomeric Equilibria. *The Journal of Physical Chemistry A* **2009**, *113*, 8434–8447.

(99) Zhao, Y.; Lynch, B. J.; Truhlar, D. G. Multi-coefficient extrapolated density functional theory for thermochemistry and thermochemical kinetics. *Phys. Chem. Chem. Phys.* **2005**, *7*, 43–52.

(100) Zhao, Y.; González-García, N.; Truhlar, D. G. Benchmark Database of Barrier Heights for Heavy Atom Transfer, Nucleophilic Substitution, Association, and Unimolecular Reactions and Its Use to Test Theoretical Methods. *The Journal of Physical Chemistry A* **2005**, *109*, 2012–2018.

(101) Thanthiriwatte, K. S.; Hohenstein, E. G.; Burns, L. A.; Sherrill, C. D. Assessment of the Performance of DFT and DFT-D Methods for Describing Distance Dependence of Hydrogen-Bonded Interactions. *Journal of Chemical Theory and Computation* **2011**, *7*, 88–96.

(102) Hohenstein, E. G.; Sherrill, C. D. Effects of Heteroatoms on Aromatic Interactions: BenzenePyridine and Pyridine Dimer. *The Journal of Physical Chemistry A* **2009**, *113*, 878–886.

(103) Gráfová, L.; Pitoňák, M.; Řezáč, J.; Hobza, P. Comparative Study of Selected Wave Function and Density Functional Methods for Noncovalent Interaction Energy Calculations Using the Extended S22 Data Set. *Journal of Chemical Theory and Computation* **2010**, *6*, 2365–2376.

(104) Řezáč, J.; Riley, K. E.; Hobza, P. S66: A Well-balanced Database of Benchmark Interaction Energies Relevant to Biomolecular Structures. *Journal of Chemical Theory and Computation* **2011**, *7*, 2427–2438.

(105) Řezáč, J.; Riley, K. E.; Hobza, P. Extensions of the S66 Data Set: More Accurate Interaction Energies and Angular-Displaced Nonequilibrium Geometries. *Journal of Chemical Theory and Computation* **2011**, *7*, 3466–3470.

(106) Tang, K. T.; Toennies, J. P. The van der Waals potentials between all the rare gas atoms from He to Rn. *The Journal of Chemical Physics* **2003**, *118*, 4976–4983.

(107) Curtiss, L. A.; Raghavachari, K.; Trucks, G. W.; Pople, J. A. Gaussian-2 theory for molecular energies of first- and second-row compounds. *The Journal of Chemical Physics* **1991**, *94*, 7221–7230.

(108) Goerigk, L.; Grimme, S. Efficient and Accurate Double-Hybrid-Meta-GGA Density FunctionalsEvaluation with the Extended GMTKN30 Database for General Main Group Thermochemistry, Kinetics, and Noncovalent Interactions. *Journal of Chemical Theory and Computation* **2011**, *7*, 291–309.

(109) Parthiban, S.; Martin, J. M. L. Assessment of W1 and W2 theories for the computation of electron affinities, ionization potentials, heats of formation, and proton affinities. *The Journal of Chemical Physics* **2001**, *114*, 6014–6029.

(110) Zhao, Y.; Truhlar, D. G. Assessment of Density Functionals for Systems: Energy Differences between Cumulenes and Poly-ynes; Proton Affinities, Bond Length Alternation, and Torsional Potentials of Conjugated Polyenes; and Proton Affinities of Conjugated Shiff Bases. *The Journal of Physical Chemistry A* **2006**, *110*, 10478–10486.

(111) Brittain, D. R. B.; Lin, C. Y.; Gilbert, A. T. B.; Izgorodina, E. I.; Gill, P. M. W.; Coote, M. L. The role of exchange in systematic DFT errors for some organic reactions. *Phys. Chem. Chem. Phys.* **2009**, *11*, 1138–1142.

(112) Řezáč, J.; Hobza, P. Describing Noncovalent Interactions beyond the Common Approximations: How Accurate Is the Gold Standard CCSD(T) at the Complete Basis Set Limit? *Journal of Chemical Theory and Computation* **2013**, *9*, 2151–2155.

(113) Řezáč, J.; Riley, K. E.; Hobza, P. Benchmark Calculations of Noncovalent Interactions of Halogenated Molecules. *Journal of Chemical Theory and Computation* **2012**, *8*, 4285–4292.

(114) Lao, K. U.; Herbert, J. M. An improved treatment of empirical dispersion and a many-body energy decomposition scheme for the explicit polarization plus symmetry-adapted perturbation theory (XSAPT) method. *The Journal of Chemical Physics* **2013**, *139*, 034107.

(115) Wilke, J. J.; Lind, M. C.; Schaefer, H. F.; Csaszar, A. G.; Allen, W. D. Conformers of Gaseous Cysteine. *Journal of Chemical Theory and Computation* **2009**, *5*, 1511–1523.

(116) Mintz, B. J.; Parks, J. M. Benchmark Interaction Energies for Biologically Relevant Noncovalent Complexes Containing Divalent Sulfur. *The Journal of Physical Chemistry A* **2012**, *116*, 1086–1092.

(117) Bryantsev, V. S.; Diallo, M. S.; van Duin, A. C. T.; Goddard, W. A. Evaluation of B3LYP, X3LYP, and M06-Class Density Functionals for Predicting the Binding Energies of Neutral, Protonated, and Deprotonated Water Clusters. *Journal of Chemical Theory and Computation* **2009**, *5*, 1016–1026.

(118) Gill, P. M.; Johnson, B. G.; Pople, J. A. A standard grid for density functional calculations. *Chemical Physics Letters* **1993**, *209*, 506 – 512.

(119) Thom H. Dunning, J. Gaussian basis sets for use in correlated molecular calculations. I. The atoms boron through neon and hydrogen. *The Journal of Chemical Physics* **1989**, *90*, 1007–1023.

(120) Woon, D. E.; Thom H. Dunning, J. Gaussian basis sets for use in correlated molecular calculations. III. The atoms aluminum through argon. *The Journal of Chemical Physics* **1993**, *98*, 1358–1371.

(121) Peterson, K. A.; Figgen, D.; Goll, E.; Stoll, H.; Dolg, M. Systematically convergent basis sets with relativistic pseudopotentials. II. Small-core pseudopotentials and correlation consistent basis sets for the post-d group 16–18 elements. *The Journal of Chemical Physics* **2003**, *119*, 11113–11123.

(122) Rappoport, D.; Furche, F. Property-optimized Gaussian basis sets for molecular response calculations. *The Journal of Chemical Physics* **2010**, *133*, 134105.

(123) Burns, L. A.; Álvaro Vázquez-Mayagoitia,; Sumpter, B. G.; Sherrill, C. D. Density-functional approaches to noncovalent interactions: A comparison of dispersion corrections (DFT-D), exchange-hole dipole moment (XDM) theory, and specialized functionals. *The Journal of Chemical Physics* **2011**, *134*, 084107.

(124) Shao, Y.; Gan, Z.; Epifanovsky, E.; Gilbert, A. T.; Wormit, M.; Kussmann, J.; Lange, A. W.; Behn, A.; Deng, J.; Feng, X. et al. Advances in molecular quantum chemistry contained in the Q-Chem 4 program package. *Molecular Physics* **2015**, *113*, 184–215.

(125) Peverati, R.; Truhlar, D. G. An improved and broadly accurate local approximation to the exchange-correlation density functional: The MN12-L functional for electronic structure calculations in chemistry and physics. *Phys. Chem. Chem. Phys.* **2012**, *14*, 13171–13174.

(126) Peverati, R.; Truhlar, D. G. Screened-exchange density functionals with broad accuracy for chemistry and solid-state physics. *Phys. Chem. Chem. Phys.* **2012**, *14*, 16187–16191.

(127) Murray, E. D.; Lee, K.; Langreth, D. C. Investigation of Exchange Energy Density Functional Accuracy for Interacting Molecules. *J. Chem. Theory Comput.* **2009**, *5*, 2754–2762.

(128) Chai, J.-D.; Head-Gordon, M. Long-range corrected hybrid density functionals with damped atom-atom dispersion corrections. *Phys. Chem. Chem. Phys.* **2008**, *10*, 6615–6620.

(129) Miliordos, E.; Apr, E.; Xantheas, S. S. Benchmark Theoretical Study of the Binding Energy in the Benzene Dimer. *The Journal of Physical Chemistry A* **2014**, *118*, 7568–7578.

(130) Mardirossian, N.; Head-Gordon, M. Characterizing and Understanding the Remarkably Slow Basis Set Convergence of Several Minnesota Density Functionals for Intermolecular Interaction Energies.

Journal of Chemical Theory and Computation **2013**, *9*, 4453–4461.

(131) Janowski, T.; Ford, A. R.; Pulay, P. Accurate correlated calculation of the intermolecular potential surface in the coronene dimer. *Molecular Physics* **2010**, *108*, 249–257.

(132) Janowski, T.; Pulay, P. A Benchmark Comparison of / and / Dispersion: the Dimers of Naphthalene and Decalin, and Coronene and Perhydrocoronene. *Journal of the American Chemical Society* **2012**, *134*, 17520–17525.

(133) Sedlak, R.; Janowski, T.; Pitoňák, M.; Řezáč, J.; Pulay, P.; Hobza, P. Accuracy of Quantum Chemical Methods for Large Noncovalent Complexes. *Journal of Chemical Theory and Computation* **2013**, *9*, 3364–3374.

(134) Manzer, S. F.; Epifanovsky, E.; Head-Gordon, M. Efficient Implementation of the Pair Atomic Resolution of the Identity Approximation for Exact Exchange for Hybrid and Range-Separated Density Functionals. *Journal of Chemical Theory and Computation* **0**, *0*, null.

(135) Goerigk, L.; Grimme, S. A General Database for Main Group Thermochemistry, Kinetics, and Noncovalent Interactions Assessment of Common and Reparameterized (meta-)GGA Density Functionals. *Journal of Chemical Theory and Computation* **2010**, *6*, 107–126.

(136) Goerigk, L.; Grimme, S. A thorough benchmark of density functional methods for general main group thermochemistry, kinetics, and noncovalent interactions. *Phys. Chem. Chem. Phys.* **2011**, *13*, 6670–6688.

(137) Anacker, T.; Friedrich, J. New accurate benchmark energies for large water clusters: DFT is better than expected. *J. Comput. Chem.* **2014**, *35*, 634–643.

(138) Fanourgakis, G. S.; Aprà, E.; Xantheas, S. S. High-level ab initio calculations for the four low-lying families of minima of (H2O)20. I. Estimates of MP2/CBS binding energies and comparison with empirical potentials. *The Journal of Chemical Physics* **2004**, *121*, 2655–2663.

(139) Yoo, S.; Aprà, E.; Zeng, X. C.; Xantheas, S. S. High-Level Ab Initio Electronic Structure Calculations of Water Clusters (H2O)16 and (H2O)17: A New Global Minimum for (H2O)16. *The Journal of Physical Chemistry Letters* **2010**, *1*, 3122–3127.

(140) Řezáč, J.; Hobza, P. Advanced Corrections of Hydrogen Bonding and Dispersion for Semiempirical Quantum Mechanical Methods. *Journal of Chemical Theory and Computation* **2012**, *8*, 141–151.

(141) Faver, J. C.; Benson, M. L.; He, X.; Roberts, B. P.; Wang, B.; Marshall, M. S.; Kennedy, M. R.; Sherrill, C. D.; Merz, K. M. Formal Estimation of Errors in Computed Absolute Interaction Energies of ProteinLigand Complexes. *Journal of Chemical Theory and Computation* **2011**, *7*, 790–797.

(142) Smith, D. G. A.; Jankowski, P.; Slawik, M.; Witek, H. A.; Patkowski, K. Basis Set Convergence of the Post-CCSD(T) Contribution to Noncovalent Interaction Energies. *Journal of Chemical Theory and Computation* **2014**, *10*, 3140–3150.

(143) Temelso, B.; Archer, K. A.; Shields, G. C. Benchmark Structures and Binding Energies of Small Water Clusters with Anharmonicity Corrections. *The Journal of Physical Chemistry A* **2011**, *115*, 12034–12046.

(144) Tentscher, P. R.; Arey, J. S. Geometries and Vibrational Frequencies of Small

Radicals: Performance of Coupled Cluster and More Approximate Methods. *Journal of Chemical Theory and Computation* **2012**, *8*, 2165–2179.

(145) Bak, K. L.; Gauss, J.; Jørgensen, P.; Olsen, J.; Helgaker, T.; Stanton, J. F. The accurate determination of molecular equilibrium structures. *The Journal of Chemical Physics* **2001**, *114*, 6548–6556.

(146) Kabsch, W. A solution for the best rotation to relate two sets of vectors. *Acta Crystallographica Section A* **1976**, *32*, 922–923.